

UCSF

UC San Francisco Electronic Theses and Dissertations

Title

Mechanical Robustness of the Mammalian Kinetochore-Microtubule Interface

Permalink

<https://escholarship.org/uc/item/92w9j6gg>

Author

Long, Alexandra

Publication Date

2020

Peer reviewed|Thesis/dissertation

Mechanical Robustness of the Mammalian Kinetochores-Microtubule Interface

by
Alexandra Long

DISSERTATION
Submitted in partial satisfaction of the requirements for degree of
DOCTOR OF PHILOSOPHY

in
Cell Biology

in the
GRADUATE DIVISION
of the
UNIVERSITY OF CALIFORNIA, SAN FRANCISCO

Approved:

DocuSigned by:
Ronald Vale Ronald Vale
A5A0784E09DA477... Chair

DocuSigned by:
Sophie Dumont Sophie Dumont

DocuSigned by:
David Morgan David Morgan

DocuSigned by:
David Agard David Agard
328308DD7E5546A...

Committee Members

Copyright 2020

by

Alexandra Long

DEDICATION

To my family, who sparked my love of learning.

ACKNOWLEDGEMENTS

I would like to thank –

- My advisor Sophie Dumont for her curiosity, kindness, and unwavering support.
- Everyone in the Dumont lab past and present – Mary Elting, Christina Hueschen, Dylan Udy, Jonathan Kuhn, Andrea Serra-Marques, Josh Guild, Meelad Amouzgar, Cynthia Chio, Clara Herrera, Lakshmi Miller-Vedam, Pooja Suresh, Lila Neahring, Manuela Richter, Miquel Rosas-Salvans, Megan Chong, Renaldo Sutanto – for their advice, creative (endless) questions and their humor.
- My early teachers and mentors who sparked my love of science: John Jannetti, Hugh Morgenbesser, Linda Doerrer, June Lum, John Tymoczko, Sabrice Guerrier, Bill Titus, Joe Chihade, Kim Woodrow, Joe Phan, Krystyn Van Vliet, and John Maloney. Thank you for having confidence in me and fostering my independence. I hope that I can pay it forward by lifting up even one student as you all have empowered me.
- The community of brilliant, creative, and generous people at UCSF and beyond who have supported and inspired me: Wallace Marshall, Mark Chan, Prachee Avasthi, Tatyana Makushok, Zev Gartner, Alec Cerciare, Rob Phillips, Nicole King, Dave Morgan, Ron Vale, David Agard, Orion Weiner, Diane Barber, Torsten Wittmann, Fred Chang, Andrei Goga, Noelle L'Etoile, Manu Prakash, Bree Grillo-Hill, Jeffrey van Haren, Katie White, Arthur Molines, Brad Webb, Dai Horiuchi, Stefan Niekamp and many others.
- The members of the Parnassus women's Peer Problem Solving Group for being my sounding board, coaches, and cheerleaders.

- The members of UCSF's Office of Career and Professional Development – especially Laurence Clement and Gabi Monsalves, Alece Alderson, Patti Meyer, and my two MIND peer groups. Thank you for showing me the many things one can do with a PhD and a process for exploring them. I am so grateful for your support and encouragement.
- My classmates and instructors in the 2016 MBL Physiology course for showing me that science is supposed to be fun and to change things up if it's not (and to always go to the beach when experiments fail).
- My friends and fellow Tetrad classmates, especially Jess, Anne, Han, Susan, as well as Frances, Delsy, Betsy, LEEanne, and Melanie for making San Francisco feel like home. It is a privilege to be a part of this group of strong women.
- My friends Laura, Katy, Anna, Jonathan, Nana, Alex, Rachel, Lingerr, Morgan, Daniel, Lydia, Rob – for being there for me for through the ups and downs.
- My family – especially my parents Dan and Denise and brother Adam – for inspiring my love of science and showing me firsthand how to push through projects and challenges that seem insurmountable. Thank you for supporting me on this journey even though it has led me so far from home.
- My husband Noah – I can't list even a fraction of the things you have done to support me. Thank you for sharing the joys of science with me, for always having confidence in me, and for reminding me about what really matters.
- Lastly, thank you to my dog Grace – whose energy and unconditional love have motivated me in these last years of grad school.

STATEMENT REGARDING AUTHOR CONTRIBUTIONS

Chapters 1 and 4 of this dissertation contain partial reprints of previously published material:

Long, A.F., Kuhn, J.A. and Dumont, S. (2019) The mammalian kinetochore-microtubule interface: robust mechanics and computation with many microtubules. *Current Opinion in Cell Biology*, 60. 60-67.

I wrote the review article that was adapted in Chapters 1 and 4 and created the figures under the guidance of Sophie Dumont, PhD. My co-author Jonathan Kuhn (UCSF) wrote one section, provided critical brainstorming about the themes, and helped edit the article.

Chapter 2 of this dissertation is a reprint of previously published material:

Long, A.F., Udy, D.B., and Dumont, S. (2017). Hec1 Tail Phosphorylation Differentially Regulates Mammalian Kinetochore Coupling to Polymerizing and Depolymerizing Microtubules. *Current Biology* 27(11). 1692-1699.

I performed the studies described in Chapter 2 under the guidance of Sophie Dumont, PhD. Dylan Udy (UCSF) performed some of the preliminary experiments and provided technical assistance.

Chapter 3 of this dissertation contains unpublished material that is under review:

Long, A.F., Suresh, P. and Dumont, S. Individual kinetochore-fibers locally dissipate force to maintain robust mammalian spindle structure. bioRxiv.

<https://doi.org/10.1101/846154>. (Manuscript under review)

I performed the studies described in Chapter 3 under the guidance of Sophie Dumont, PhD. Pooja Suresh (UCSF) assisted with technical development of the microneedle manipulation assays and quantification.

ABSTRACT

Mechanical Robustness of the Mammalian Kinetochore-Microtubule Interface

Alexandra Long

For a cell to divide correctly, the spindle must connect to and align chromosomes and then generate force to move them into two daughter cells. The kinetochore is the macromolecular machine that connects chromosomes to a bundle of dynamic microtubules, the kinetochore-fiber (k-fiber). While we have a nearly complete parts list of kinetochore components and regulators, how they together give rise to the robust mechanics of the kinetochore-microtubule interface remains poorly understood. This is due to the fact that mammalian kinetochores and k-fibers cannot yet be reconstituted *in vitro* and there are few tools to perturb forces and measure the mechanics at this interface *in vivo*. In my thesis work I have addressed this gap using direct biophysical assays in mammalian cells to focus on two main questions about the kinetochore-microtubule interface. First, how do kinetochores hold on to microtubules that grow and shrink? Using live imaging to monitor spindle dynamics and laser ablation to challenge kinetochore grip, I show that regulation of the key microtubule binding protein Ndc80/Hec1 at the outer kinetochore by the kinase Aurora B specifically affects kinetochore movement on polymerizing microtubules without disrupting coupling to depolymerizing microtubules that generate force to move chromosomes. Second, at the other side of the interface, how do kinetochore-fibers remodel under force? I directly exert forces on individual mammalian k-fibers and find that even under high force for minutes they do not lose grip. Instead, k-fibers bend and elongate by polymerizing at

normal rates at plus-ends and inhibiting depolymerization at minus-ends – thus ensuring robust connection to kinetochores. Altogether I find that robust kinetochore grip emerges from underlying properties of both the kinetochore and k-fiber microtubules – specialized regulation at the kinetochore allows the cell to adjust grip while still allowing force generation and dynamic mechanical feedback of k-fiber microtubules locally dissipates force, protecting spindle connections. These fundamental physical properties of the kinetochore-microtubule interface allow the spindle to faithfully segregate chromosomes and more broadly suggest a model for how force-generating cellular machines can also robustly maintain their structure.

TABLE OF CONTENTS

CHAPTER 1 INTRODUCTION	1
FORCE GENERATION BY BIOLOGICAL STRUCTURES	2
PRINCIPLES OF ROBUST KINETOCHORE GRIP	4
OBJECTIVES OF THESIS	8
FIGURES AND FIGURE LEGENDS	10
CHAPTER 2 HEC1 TAIL PHOSPHORYLATION DIFFERENTIALLY REGULATES MAMMALIAN KINETOCHORE COUPLING TO POLYMERIZING AND DEPOLYMERIZING MICROTUBULES	12
SUMMARY	13
RESULTS	14
DISCUSSION	19
FIGURES AND FIGURE LEGENDS	22
MATERIALS AND METHODS	30
ACKNOWLEDGEMENTS	34
CHAPTER 3 INDIVIDUAL KINETOCHORE-FIBERS LOCALLY DISSIPATE FORCE TO MAINTAIN ROBUST MAMMALIAN SPINDLE STRUCTURE	36
ABSTRACT	37
INTRODUCTION.....	37
RESULTS.....	40
DISCUSSION.....	46

FIGURES AND FIGURE LEGENDS	50
MATERIALS AND METHODS.....	58
ACKNOWLEDGEMENTS	65
CHAPTER 4 CONCLUSION.....	67
EMERGENT MECHANICS OF THE KINETOCHORE-MICROTUBULE INTERFACE.....	68
MECHANICAL INSIGHTS ACROSS SPECIES	70
NEW TOOLS AND APPROACHES.....	71
REFERENCES.....	72

LIST OF FIGURES

CHAPTER 1

FIGURE 1.1.....	10
FIGURE 1.2.....	11

CHAPTER 2

FIGURE 2.1.....	22
FIGURE 2.2.....	24
FIGURE 2.3.....	25
FIGURE S2.1	27

CHAPTER 3

FIGURE 3.1.....	50
FIGURE 3.2.....	51
FIGURE 3.3.....	53
FIGURE 3.4.....	55
FIGURE 3.5.....	57

LIST OF TABLES

CHAPTER 2

TABLE 2.1.....	28
----------------	----

CHAPTER ONE

INTRODUCTION

FORCE GENERATION BY BIOLOGICAL STRUCTURES

Life, at many scales, is a mechanical process. Redwoods unfurl their leaves, animals sprint, and fungi branch networks deep into the soil. These activities are powered by the sophisticated dynamics of the machinery within individual cells. Inside a cell is a blur of activity – proteins are synthesized and recycled, molecular motors move internal cargo – all the while the cell itself can perform an integrated mechanical function such as crawling through a complex environment or dividing in two. How do these mechanical behaviors at the micron-scale emerge from the behavior of nanometer-scale components? With all these mechanical activities occurring within and around cells, how do they both generate and respond to forces as cues, while also remaining intact? To address these key questions, in my thesis work I have used the mammalian mitotic spindle as a model system to study how cellular machines can actively generate force for critical cellular behaviors while remaining one mechanically robust structure.

Each time a cell divides, the mitotic spindle generates force to align and then segregate the chromosomes to two new daughter cells. Chromosome movement is powered by the growing and shrinking of dynamic microtubule (MT) polymers that connect to chromosomes via a macromolecular complex called the kinetochore. For genomic information to be accurately segregated and preserved as cells divide, the attachment of chromosomes to the spindle must be both robust and correct. Weak or erroneous kinetochore attachments can lead to aneuploid cells that lack a correct copy of the genome, which can lead to birth defects [1] and are a hallmark of cancer [2]. Thus, the kinetochore plays key physical and signaling roles: it must grip spindle

microtubules while still allowing them to be dynamic, and must also process attachment information to signal when chromosome separation can begin.

The mammalian kinetochore is built from ~100 protein species present in many copies in a well-defined stoichiometry, and it binds the 15-25 microtubules that make up the kinetochore-fiber (k-fiber) [3,4] (Fig. 1.1). We now have a near complete parts list for the mammalian kinetochore, and there are significant efforts to map the stoichiometry, structure and biochemistry of this macromolecular machine [4–7]. Yet, how this machine's mechanical functions emerge from its component parts has long remained a frontier because of the system's complexity and since mammalian kinetochores and k-fibers cannot yet be reconstituted *in vitro*. Expanding physical and molecular toolboxes in cells are now helping us address this question, which is the central topic of this thesis.

First, in this introductory chapter I review our current understanding of how the mammalian kinetochore's individual parts together, as an ensemble, give rise to some of its key mechanical functions as it binds the k-fiber's many microtubules (Fig. 1.1). Then in the chapters of this thesis that follow I address two key questions about mechanics of the kinetochore-microtubule interface. In Chapter 2 I ask: how do kinetochores grip multiple microtubules to maintain attachments that are mechanically strong, and yet flexible enough to allow microtubules to grow and shrink and detach to correct errors? In Chapter 3 I ask: how do dynamic kinetochore-fibers generate, respond to, and withstand force to move chromosomes? Lastly in Chapter 4, I discuss open questions about the emergent mechanics of the kinetochore-microtubule interface, and new tools and conceptual approaches with which to tackle them in the future.

PRINCIPLES OF ROBUST KINETOCHORE GRIP

The inner kinetochore assembles on centromeric chromatin while the outer kinetochore forms the microtubule binding and signaling platform [7,8]. During microtubule attachment, outer kinetochore modules undergo structural rearrangements thought to aid in efficient spindle assembly [9–12]. Kinetochores face a challenging task: if they bind too tightly to microtubules, they avoid detachment but may disrupt microtubule dynamics (growth and shrinkage) or stabilize incorrect attachments, yet if they bind too loosely, they may not be able to correctly move chromosomes into each daughter cell. The kinetochore-microtubule interface must therefore be tuned to achieve robust and dynamic, not just strong, binding. Diverse architectural features of this interface are well-suited to facilitate robust grip (Fig. 1.2): many outer kinetochore proteins work together to bind many microtubules in a k-fiber (*redundancy*), a diversity of kinetochore proteins likely contribute to load-bearing (*specialization*), the mechanics of the interface can be regulated to adjust grip as needed (*tunability*) and k-fiber microtubules can grow and shrink (*dynamicity*), generating force to move chromosomes and allowing the spindle to remodel itself. I provide key examples of these features below, focusing on recent work.

Redundancy

Redundancy is a hallmark of the mammalian kinetochore-microtubule interface. I use ‘redundancy’ to emphasize the multiplicity of components, where each and every

copy may not be necessary. The kinetochore's main load-bearing microtubule binding unit, the Ndc80 complex [13,14], has ~250 copies per kinetochore (Fig. 1.2) [15], of which only a low fraction (~30%) are engaged with microtubules [16] at any given time during metaphase. Redundancy at the level of kinetochore protein structure (e.g. a single protein may have multiple binding surfaces [17]) or sub-complex architecture (e.g. the multivalent arrangement of couplers [18]) may also be critical for robust tracking of dynamic microtubules by providing multiple contact points. At the kinetochore-microtubule interface, redundancy also occurs at the level of many microtubules (Fig. 1.2). Many microtubules compose the mature k-fiber, exceeding the minimum number required for SAC satisfaction [19,20] and the estimated number needed to generate force to move a chromosome [21,22]. The high number of bound microtubules may instead ensure robust segregation by ensuring that turnover of k-fiber microtubules or error correction activities – both essential to function – do not fully disconnect a kinetochore from the spindle [19]. Further, having many redundant kinetochore coupling points may provide more sites for cellular regulation to tune microtubule affinity [23].

Specialization

Not only do kinetochore proteins play highly specialized biochemical roles, they also play specialized mechanical roles in microtubule binding (Fig. 1.2). Some of these proteins may be regulated to correct errors or stabilize proper attachments as mitosis progresses. Defining the specific mechanical functions and relative contributions of

different proteins to the mechanics of the kinetochore-microtubule interface is critical for understanding kinetochore structure-function. Several proteins act in kinetochore-microtubule attachment in addition to the Ndc80 complex. For example, proteins such as the Ska complex [24–27], Cdt1 [28] and astrin-SKAP [29] have been proposed to act as additional couplers between kinetochores and microtubules, perhaps as “lock-down” factors [25]. Notably, many of these modules’ grip is regulated by the same set of kinases and phosphatases (tunability), which may ensure that whole kinetochore mechanics can be tuned as one ensemble (Fig. 1.2) [28,30–32]. Specialization in grip may also arise from the same outer kinetochore protein complexes engaging differently either in structure or in number with growing versus shrinking microtubules (Fig. 1.2) [16,33]. Determining which protein modules map to sites of active (energy consuming) and passive (non-energy consuming, e.g. frictional) force generation at the kinetochore-microtubule interface [34]. Just as ascribing specific biochemical functions to kinetochore proteins has helped us understand the mechanisms of kinetochore signaling, mapping specific mechanical functions to diverse proteins is key for us to understand the underlying engineering principles that drive the kinetochore’s robust grip.

Dynamicity

Robust grip is not only determined by kinetochore composition and architecture, but also by the k-fiber’s dynamicity (Fig. 1.2). K-fiber shrinkage powers chromosome movement [22] and k-fiber growth allows movement of the paired sister kinetochore.

Thus it is key for the cell to limit growth and shrinkage velocities [35,36], to ensure that shrinking microtubules can move chromosomes on relevant timescales, and that kinetochores can keep track of microtubule ends without losing grip. Plus-end dynamics of individual microtubules within the kinetochore must also be coordinated [37]. An ensemble of regulatory proteins limits the dynamic range of microtubule growth and shrinkage, and imbalance of these regulators can lead to mitotic errors [38,39]. Further, just as microtubule dynamics can generate mechanical force, they are also regulated by force. The ability of force (in a given regime) to stabilize attachments has been directly shown and mapped at the reconstituted budding yeast kinetochore [40] and at grasshopper kinetochores inside cells [21,41], but we still lack a direct and quantitative understanding of this mechanical feedback at the mammalian kinetochore, which we explore in chapter 3 of this thesis. In principle, the ability of microtubule dynamics to respond to force is well suited to help dissipate force across the spindle, providing 'slack' in the system [42]. Flux of k-fiber microtubules towards spindle poles may play a similar role [42–44], and could also enhance kinetochore binding by biasing k-fibers towards a growing state where kinetochores may have specialized engagement [16]. In addition to microtubule end dynamics, the lifetime of components of the kinetochore-microtubule interface must also drive the interface's mechanical function [45]. For example, the engagement between individual Ndc80 complexes and the microtubule is highly transient, which may allow rapid interface dynamics, while the longer lifetime of k-fiber microtubules is well-suited to ensure that correct microtubule attachments are stable.

OBJECTIVES OF THESIS

In this dissertation I use the kinetochore-microtubule interface of the mitotic spindle as a model system to address core questions about how cellular machines generate, respond to, and withstand force. This is an ideal system in which to study these processes as it has a near-complete molecular parts list and performs an essential mechanical function for the cell:

"... through extensive trial and error, nature has chosen an intricately interacting, dynamic system to achieve mitosis, and to safeguard the propagation and unfolding of life despite its myriad forms. While we are becoming privy to some of nature's surprising ways today, we need, in addition to dissecting the molecules further, to listen ever more carefully to the living cell, and be prepared to be taught further unexpected paradigms, which will undoubtedly be essential for clearer understanding of the physico-chemical and biological basis of cellular organization, life, and disease" - S. Inoue and E. Salmon [46]

The objective of this work is to harness old and new top-down physical approaches and microscopy to better “listen” to the living cell to gain insight into how its mechanical behaviors emerge from its underlying molecular parts. Using these direct physical approaches inside mammalian cells, I quantitatively examine how the kinetochore-microtubule interface performs its robust mechanical functions. In chapter 2, I find that cells can differentially regulate the protein Ndc80 to adjust grip in a mechanically specialized manner without compromising force generation. In chapter 3, I find that the dynamicity of the many redundant microtubules of the mammalian k-fiber allow it to respond to and dissipate mechanical force to maintain robust connection to the kinetochore. Together, these key engineering principles enable the kinetochore-microtubule interface to generate and respond to cellular forces while maintaining

robust connectivity to ensure proper chromosome segregation. These underlying principles will be broadly relevant for understanding diverse force-generating cellular machines that perform important cellular processes.

FIGURES AND FIGURE LEGENDS

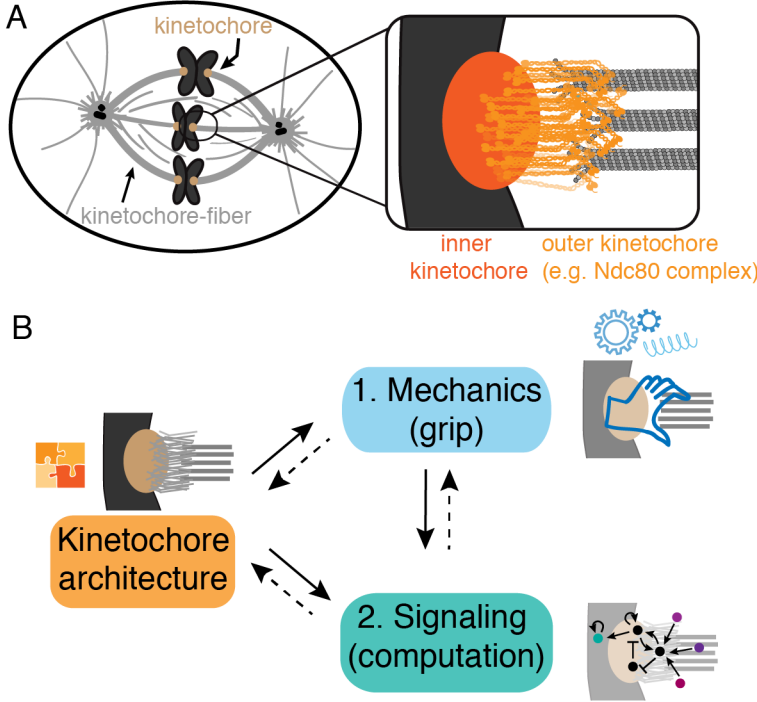


Figure 1.1. The mammalian kinetochore-microtubule interface.

A) Mammalian kinetochores (brown) connect chromosomes (dark gray) to kinetochore-fibers (“k-fibers”, light gray), bundles of many microtubules. In the inset, the outer kinetochore (light orange, e.g. Ndc80 complexes depicted) is a lawn of proteins that form the microtubule-interacting interface. The inner kinetochore (dark orange) links the outer kinetochore to centromeric chromatin.

B) Kinetochore architecture, mechanics and signaling nodes feed back on each other to give rise to robust kinetochore function. In this chapter, I highlight (solid arrows) how the specific molecular interactions and architecture (orange puzzle pieces) gives rise to robust grip (blue).

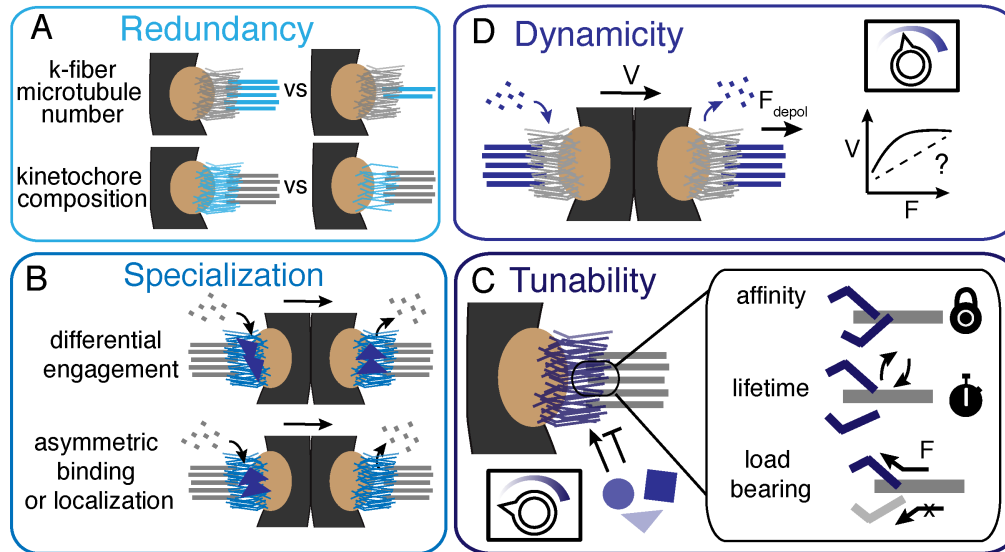


Figure 1.2. Principles of robust grip at the mammalian kinetochore-microtubule interface.

A) Redundancy occurs at multiple levels. For example, many microtubules in the kinetochore-fiber (top) bind a single mammalian kinetochore, and many kinetochore protein copies bind a single microtubule (bottom).

B) Kinetochore specialization in binding growing (left) versus shrinking (right) microtubules can occur via differential engagement of kinetochore proteins (top) or via differential localization or regulation of proteins (bottom).

C) Tunability of the kinetochore-microtubule interface occurs via diverse regulators including kinases and phosphatases, plus-tip proteins and the binding of different kinetochore proteins over time during mitosis, acting on either kinetochore proteins or k-fiber microtubules. Inset shows examples of three different facets of kinetochore-microtubule interactions that can be tuned by the cell.

D) Dynamicity at the kinetochore-microtubule interface occurs from microtubule growth and shrinkage, and it is modulated by a complex network of positive and negative regulators that tune microtubule dynamics and thereby kinetochore velocity. Inset shows potential models for how force at this interface affects microtubule growth or shrinkage velocity, i.e. the force-velocity relationship of this interface.

CHAPTER TWO

HEC1 TAIL PHOSPHORYLATION DIFFERENTIALLY REGULATES MAMMALIAN KINETOCHORE COUPLING TO POLYMERIZING AND DEPOLYMERIZING MICROTUBULES

SUMMARY

The kinetochore links chromosomes to dynamic spindle microtubules and drives both chromosome congression and segregation. To do so, the kinetochore must hold on to depolymerizing and polymerizing microtubules. At metaphase, one sister kinetochore couples to depolymerizing microtubules, pulling its sister along polymerizing microtubules [47,48]. Distinct kinetochore-microtubule interfaces mediate these behaviors: active interfaces transduce microtubule depolymerization into mechanical work, and passive interfaces generate friction as the kinetochore moves along microtubules [42,49]. Despite a growing understanding of the molecular components that mediate kinetochore binding [50–52], we do not know how kinetochores physically interact with polymerizing versus depolymerizing microtubule bundles, and whether they use the same mechanisms and regulation to do so. To address this question, we focus on the mechanical role of the essential load-bearing protein Hec1 [13,14,53,54]. Hec1's affinity for microtubules is regulated by Aurora B phosphorylation on its N-terminal tail [23,30,55,56], but its role at the interface with polymerizing versus depolymerizing microtubules remains unclear. Here, we use laser ablation to trigger cellular pulling on mutant kinetochores and decouple sisters *in vivo*, and thereby separately probe Hec1's role on polymerizing versus depolymerizing microtubules. We show that Hec1 tail phosphorylation tunes friction along polymerizing microtubules, modulating both the magnitude and timescale of responses to force. In contrast, we find that Hec1 tail phosphorylation does not affect the kinetochore's ability to grip depolymerizing microtubules, or switch to this active force-generating state. Together, the data suggest that kinetochore regulation may have differential effects on how kinetochores engage

with growing and shrinking microtubules, and that friction can be regulated without disrupting active force generation. Through this mechanism, the kinetochore can modulate its grip on microtubules as its functional needs change during mitosis, and yet retain its ability to couple to microtubules powering chromosome movement.

RESULTS

Targeted control of cellular pulling forces on kinetochores in vivo

To probe Hec1's mechanical role at the mammalian kinetochore-microtubule interface, we sought the ability to exert force on a given kinetochore inside a cell at a specific time. This is necessary to probe the magnitude and timescale of a kinetochore's response to force, and to perturb kinetochores moving on microtubules in a given polymerization state. We accomplished this using targeted laser ablation to sever one kinetochore-fiber (k-fiber) at metaphase (Fig. 2.1A). The newly created k-fiber minus-ends recruit dynein, which in turn exerts a poleward pulling force on the attached kinetochore and its sister [57,58].

As a starting point for our Hec1 studies, we expressed Hec1-EGFP in PtK2 cells depleted of endogenous Hec1 by RNAi [54]. We selectively severed polymerizing k-fibers near their kinetochore, and examined the responses of both the "front" and "back" sister kinetochores (proximal and distal to the cut, respectively) (Fig. 2.1A,B). The response to laser ablation appeared the same as in wild type cells [57,58], and had two phases (Fig. 2.1B,E-G blue traces; Table 2.1; n=13). First, the front kinetochore recoiled

immediately after cut, reflecting a decrease in force and causing the interkinetochore (K-K) distance to decrease. Second, dynein pulled the microtubules bound to the front kinetochore, moving the sister pair toward the ablation site and increasing the K-K distance. Dynein pulled the front sister faster than its k-fiber polymerized or depolymerized, and faster than normal metaphase movements [57] (Table 2.1). The front kinetochore's velocity during dynein-mediated movement was similar between experiments (Fig. 2.1F,H blue traces; Table 2.1), consistent with ablation triggering a consistent response. Dynein pulling caused the back kinetochore to turn around within seconds, ultimately pulling it away from its pole along polymerizing microtubules. Thus, targeted k-fiber ablation can produce a pulling force to probe the mechanics of the interface between kinetochores and polymerizing microtubules.

Hec1 tail phosphorylation regulates the magnitude and timescale of the mammalian kinetochore-microtubule interface's response to force

To probe the mechanical regulation conferred by Hec1's N-terminal tail phosphorylation during mitosis, we asked whether and how it controls the movement of a kinetochore in response to force. We depleted endogenous Hec1 by RNAi (Fig. S2.1), and expressed either Hec1-9A-EGFP or Hec1-9D-EGFP to mimic constitutive dephosphorylation and phosphorylation, respectively, a range that includes typical Hec1 phosphorylation by Aurora B during mitosis [23]. As expected [23], Hec1-9D and Hec1-9A kinetochores resulted in different steady-state K-K distances (Fig. 2.1C,D,G; Table 2.1).

We subjected these Hec1-9A (Fig. 2.1E-G red traces; n=17) and Hec1-9D kinetochores (Fig. 2.1E-G, green traces; n=10) to the same force signature as Hec1-WT, as suggested by similar front kinetochore velocities during dynein pulling (Fig. 2.1H, Table 2.1). As with Hec1-WT, after k-fiber ablation the front kinetochore recoiled and the K-K distance decreased in both Hec1-9A and Hec1-9D cells. When dynein pulling engaged, however, the back sister responses were different from Hec1-WT. In Hec1-9A cells, the back kinetochore moved more slowly than its front sister (0.6 ± 0.1 vs $1.6 \pm 0.2 \mu\text{m}/\text{min}$; Table 2.1), and moved less far than Hec1-WT (0.4 ± 0.1 vs $0.7 \pm 0.1 \mu\text{m}$; Fig. 2.1H,I; Table 2.1). These differences led to a larger, and longer-lasting, increase in K-K distance above baseline during dynein pulling compared to Hec1-WT (maximum K-K distance was at 95 ± 7 vs 47 ± 5 s; Fig. 2.1G; Table 2.1). In contrast, in Hec1-9D cells the back sister followed at a rate similar to its front sister (1.7 ± 0.4 vs $1.8 \pm 0.2 \mu\text{m}/\text{min}$), which is faster than Hec1-WT ($0.9 \pm 0.1 \mu\text{m}/\text{min}$), and moved farther than Hec1-WT (1.0 ± 0.2 vs $0.7 \pm 0.1 \mu\text{m}$; Fig. 2.1H,I; Table 2.1). These responses led to little overshoot in K-K distance above baseline during dynein pulling (Fig. 2.1G).

Dephosphorylating the Hec1 tail makes the back kinetochore less mobile in response to force: the back kinetochore moves more slowly and a shorter distance, and takes longer to recover, despite being under higher forces. Phosphorylating the Hec1 tail has the opposite consequences. Thus, Hec1 tail phosphorylation controls both the magnitude and timescale of the back kinetochore's response to spindle forces, and thereby sets the effective elasticity and viscosity of the spindle's reorganization in response to force. Hec1 phosphorylation regulates the back kinetochore's ability to move when bound to polymerizing microtubules under force. It could do so by directly

changing friction on the microtubule lattice, or produce an apparent change in friction by setting the polymerization dynamics at the microtubule tip.

Hec1 tail phosphorylation regulates kinetochore friction on polymerizing microtubules

To probe the relationship between Hec1 tail phosphorylation and friction, we measured how Hec1 tail phosphorylation changes the velocity – and friction coefficient assuming similar forces – between kinetochore and polymerizing microtubules. To determine kinetochore velocity relative to the microtubule lattice, we tracked kinetochores with Hec1-EGFP phosphomutants, and concurrently measured k-fiber poleward flux [59] by either photomarking PA-GFP-tubulin or photobleaching GFP-tubulin (Fig. 2.2A-C). K-fiber flux velocities were lower in Hec1-9A ($0.50 \pm 0.03 \mu\text{m}/\text{min}$, $n=60$) than in Hec1-9D ($0.73 \pm 0.07 \mu\text{m}/\text{min}$, $n=27$) or WT cells ($0.65 \pm 0.05 \mu\text{m}/\text{min}$, $n=57$) although spindle length did not change (Fig. 2.2D,E, Table 2.1). Consistent with Hec1 tail phosphorylation decreasing friction, kinetochore velocity with respect to the microtubule lattice during polymerization was higher in Hec1-WT ($1.20 \pm 0.03 \mu\text{m}/\text{min}$, $n=720$) than in Hec1-9A cells ($0.80 \pm 0.03 \mu\text{m}/\text{min}$, $n=940$) (Fig. 2.2F, Table 2.1). Thus, the interface remains dynamic and is never locked within the cell's Hec1 tail phosphorylation range; the kinetochore (as a “slip clutch” [42]) can always slip to reduce force on the chromosome – and prevent detachment from microtubules [43].

These data are consistent with Hec1 being a component of a frictional interface of kinetochores with microtubules – whose location was inferred to be in the outer kinetochore [34]. Hec1 tail phosphorylation is well-suited to tune the effective friction

coefficient, and thus the force-velocity relationship, between the mammalian kinetochore and microtubules during polymerization, and to do so in a force range relevant to spindle function.

Hec1 tail phosphorylation does not disrupt the mammalian kinetochore's ability to couple to depolymerizing microtubules

As we found that Hec1 tail phosphorylation decreases kinetochore friction with microtubules during polymerization (Fig. 2.1-2), we asked whether it also affects the ability to couple to depolymerizing microtubules. Perturbing Hec1 phosphoregulation changes how metaphase sister kinetochores move [13,14], but when sister kinetochores are linked (Fig. 2.1-2), the coupling to depolymerizing microtubules can never be probed directly as it is always resisted by its sister. Anaphase kinetochores could provide a solution, but kinetochore biochemistry changes between metaphase and anaphase [60]. Hence, we turned to laser ablation to physically separate sister kinetochores: after ablating one sister, the remaining sister moves towards its pole as its k-fiber depolymerizes [47,61] (Fig. 2.3A,B).

After sister ablation, Hec1-WT kinetochores initially moving poleward speed up, from $1.2 \pm 0.2 \mu\text{m}/\text{min}$ (depolymerizing microtubules since faster than tubulin flux, Fig. 2.2D) to $2.3 \pm 0.2 \mu\text{m}/\text{min}$ ($n=10$, $p<0.01$; Fig. 2.3C,D). This acceleration is consistent with the sister, bound to polymerizing microtubules before ablation, providing resistance. In turn, WT kinetochores initially moving away from their pole (polymerizing microtubules) at $0.7 \pm 0.1 \mu\text{m}/\text{min}$ switch to poleward movement at $2.1 \pm 0.1 \mu\text{m}/\text{min}$ ($n=14$; Fig. 2.3C,D).

The directional switch and kinetochore velocity we measure here are faster than those we measured after k-fiber ablation (Fig. 2.1), which is likely because here there is no resistance from the sister k-fiber interacting with the spindle. Surprisingly, Hec1-9A and Hec1-9D kinetochores, which had perturbed K-K distances (Table 2.1), moved poleward at the same velocity as Hec1-WT after sister ablation ($2.0 \pm 0.2 \mu\text{m}/\text{min}$, $n=21$ and $2.3 \pm 0.2 \mu\text{m}/\text{min}$, $n=18$, respectively; Fig. 2.3B,E,F). As kinetochores approach poles, kinetochore velocity remained unchanged despite chromosomes experiencing higher polar ejection forces [61,62]. Although more data would be needed to make a stronger statement, we found that, within our $\sim 2\text{s}$ resolution, the different Hec1 phosphomutants had indistinguishable times to switch directions – suggesting that Hec1 tail phosphorylation may not directly regulate the kinetochore directional switching (Fig. 2.3G,H). Thus, while Hec1 tail phosphorylation regulates the kinetochore's ability to couple to polymerizing microtubules (Fig. 2.1-2), it does not affect its ability to couple to and track depolymerizing microtubules or its poleward velocity (Fig. 2.3).

DISCUSSION

Accurate chromosome segregation requires the kinetochore to be able to hold on to both polymerizing and depolymerizing microtubules. However, the molecular basis and regulation of kinetochore attachment to polymerizing and depolymerizing k-fibers are not known. In particular, separately probing kinetochore movement in defined polymerization states has been challenging. Elegant *in vitro* assays [40,63] overcome these challenges but are not yet tractable for mammalian kinetochores, while *in vivo* microneedle [64,65] and laser ablation [47,61,66] studies have probed kinetochore

mechanics in defined states, but not their molecular basis. Here, we use a combination of molecular and mechanical perturbations to determine the contribution of Hec1 tail phosphoregulation to mammalian kinetochore movement on polymerizing and depolymerizing microtubules. We find that through Hec1 tail phosphorylation, the kinetochore can independently regulate its ability to move when bound to polymerizing microtubules without losing its ability to couple to depolymerizing microtubules that actively move chromosomes (Fig. 2.3I,J). As the needs of mitosis change, regulation of effective kinetochore friction may set how far and how fast chromosomes move in response to force, and tune whole spindle mechanics, for example increasing mechanical coupling across spindle halves as mitosis progresses.

The basis for Hec1's tail regulating kinetochore movement when bound to polymerizing but not depolymerizing microtubules is not known. If kinetochore speeds were higher during polymerization than depolymerization states, changes in friction may only be detectable during polymerization; however, we observe higher speeds during depolymerization (Fig. 2.3I, Table 2.1). Similarly, direction-specific regulation could in principle arise from differences in microtubule plus-end tip structure, but this structure so far appears not to differ between sisters [67]. Alternatively, Hec1 structure may vary when bound to polymerizing versus depolymerizing microtubules [68,69], or proteins other than Hec1 may bear load and govern chromosome velocity during depolymerization [21,46]. To uncover the molecular basis for Hec1 tail phosphorylation's direction-dependent role, it will be essential to determine whether such phosphorylation regulates friction directly (by changing the tail's microtubule affinity) or indirectly (by changing how its other domains, or other proteins, interact with

microtubules), and whether and how it affects k-fiber microtubule dynamics. Further, it will be essential to map which proteins are important for active force generation at the interface with depolymerizing microtubules.

Our work indicates that Hec1 tail phosphorylation regulates the mechanics of the mammalian kinetochore-microtubule interface in a direction-dependent manner, revealing a new level of regulation. Hec1 tail phosphorylation may impact mechanics and regulate microtubule dynamics in both directions *in vitro* when it is the only coupler [70], but only impact them in polymerization *in vivo* due to the presence of – and load-sharing by – other microtubule binding proteins *in vivo*. Consistent with this idea, the Ndc80 tail is nonessential for movement in either direction in budding yeast [71,72], likely because both Ndc80 and the Dam1 complexes bind microtubules [73,74] and provide friction during polymerization, and Dam1 is the main coupler during depolymerization [71]. Functional homologues to Dam1 are being proposed in other eukaryotes [75,76], and the assay we develop here should be helpful in dissecting the mechanical role of these and other proteins in the active and passive force-generating microtubule interfaces of the mammalian kinetochore. Probing the relative importance of different kinetochore couplers at both interfaces will be critical to understanding the mechanical diversity of kinetochore proteins and functions across systems.

FIGURES AND FIGURE LEGENDS

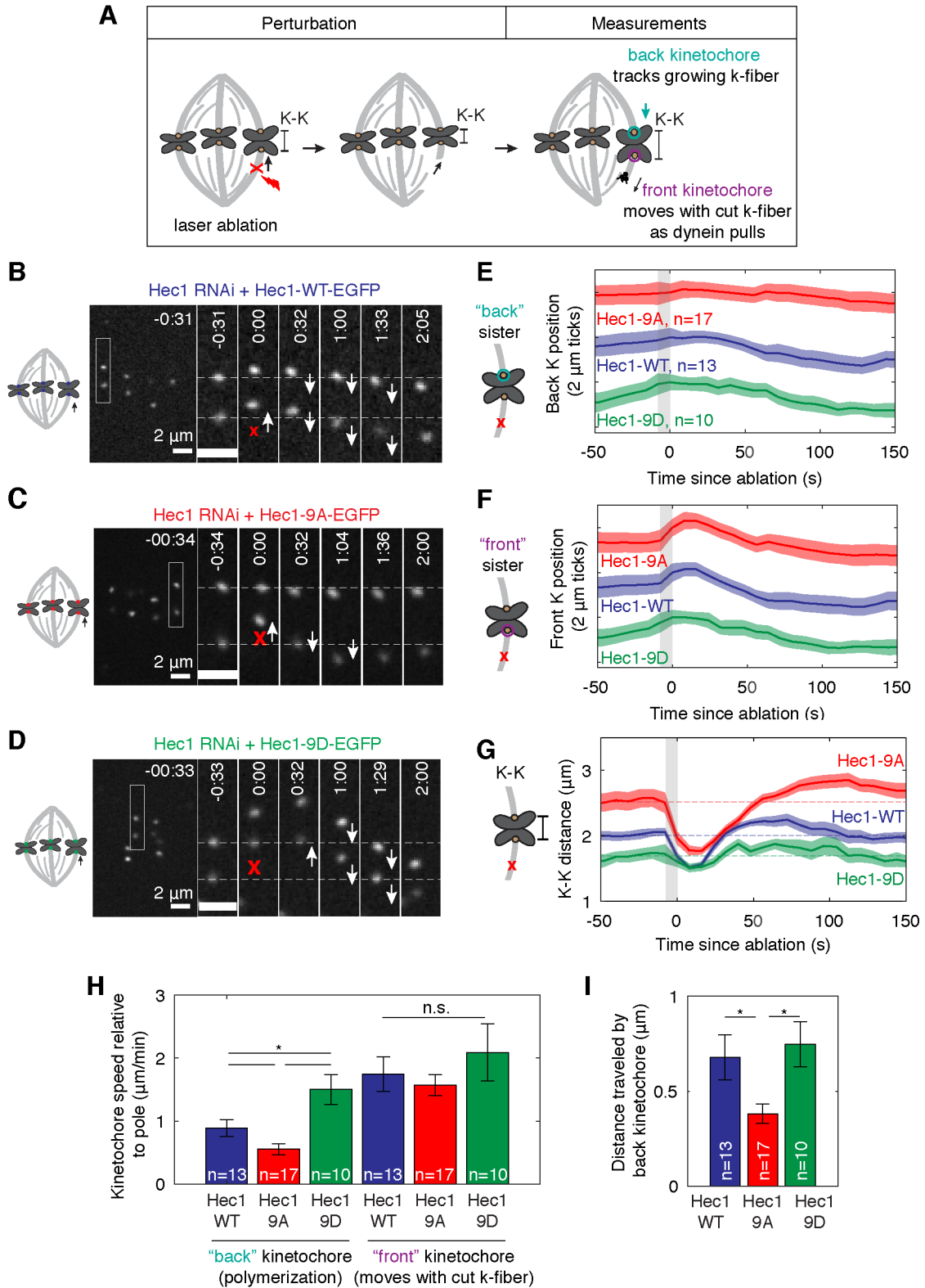


Figure 2.1 Hec1 tail phosphorylation regulates the magnitude and timescale of the mammalian kinetochore-microtubule interface's response to force.

A) Assay to sever a k-fiber using laser ablation (red X) to induce a dynein-based poleward pulling force on a specific kinetochore pair to probe the back kinetochore's movement on polymerizing microtubules in response to force.

B-D) Timelapse showing representative response of PtK2 **(B)** Hec1-WT-EGFP, **(C)** Hec1-9A-EGFP and **(D)** Hec1-9D-EGFP (each in Hec1 RNAi background – see also Fig. S1) kinetochore pairs to k-fiber laser ablation. First frame after ablation set to 0:00.

E-G) Mean positions of Hec1-WT, Hec1-9A, and Hec1-9D **(E)** back and **(F)** front kinetochores and **(G)** K-K distance before and after laser ablation. Kinetochore position is shown normalized to its pre-ablation position. Traces are mean \pm SEM and are offset vertically for clarity in **(E,F)**.

H) Velocity of the front and back kinetochores (from **E,F**) relative to the ablation-proximal spindle pole after the directional switch to poleward motion in response to ablation, until each kinetochore returned to motion away from that pole (* for $p < 0.05$, n.s. not significant, Student's T-test).

I) Distance traveled by the back kinetochore over the first 30s of poleward motion after ablation (* for $p < 0.05$, Student's T-test). See also Figure S2.1.

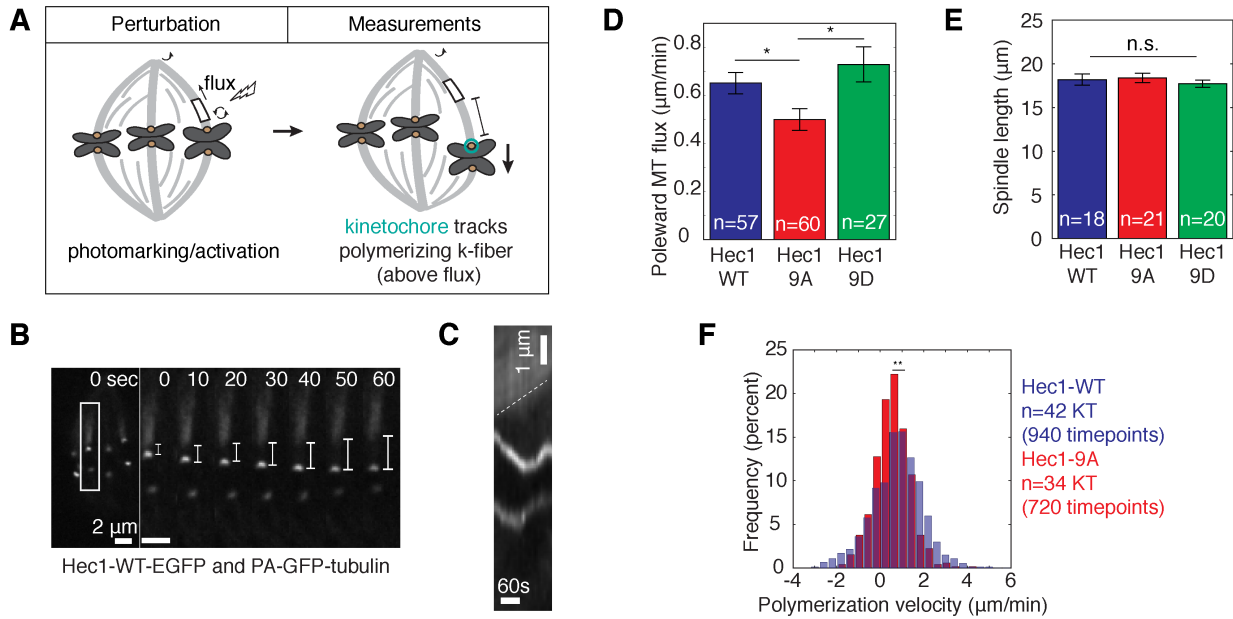


Figure 2.2 Hec1 tail phosphorylation regulates friction on kinetochores bound to polymerizing microtubules.

A) Assay to measure kinetochore velocity relative to the microtubule lattice, tracking kinetochores and poleward k-fiber microtubule flux by photomarking.

B) Representative timelapses of Hec1-EGFP and PA-GFP-tubulin PtK2 cells in a Hec1 RNAi background and **C)** kymograph of poleward microtubule flux (dotted line) measured by photoactivation. Time 0:00 corresponds to photoactivation. The distance between the photomark and the kinetochore (ruler) provides velocity relative to the microtubule lattice.

D) Microtubule flux rate (mean \pm SEM, * for $p < 0.05$, Student's T-test) in cells with Hec1-WT, Hec1-9A, or Hec1-9D kinetochores (n = number of k-fibers).

E) Histogram of kinetochore velocity relative to the microtubule lattice (** for $p < 0.01$, Student's T-test). Hec1-9D kinetochore oscillations were too variable to quantify (see Supplement).

F) Spindle length (mean \pm SEM, n.s. for not significant, $p = 0.76$ one-way ANOVA) in cells with Hec1-WT, Hec1-9A, or Hec1-9D kinetochores (n = number of cells).

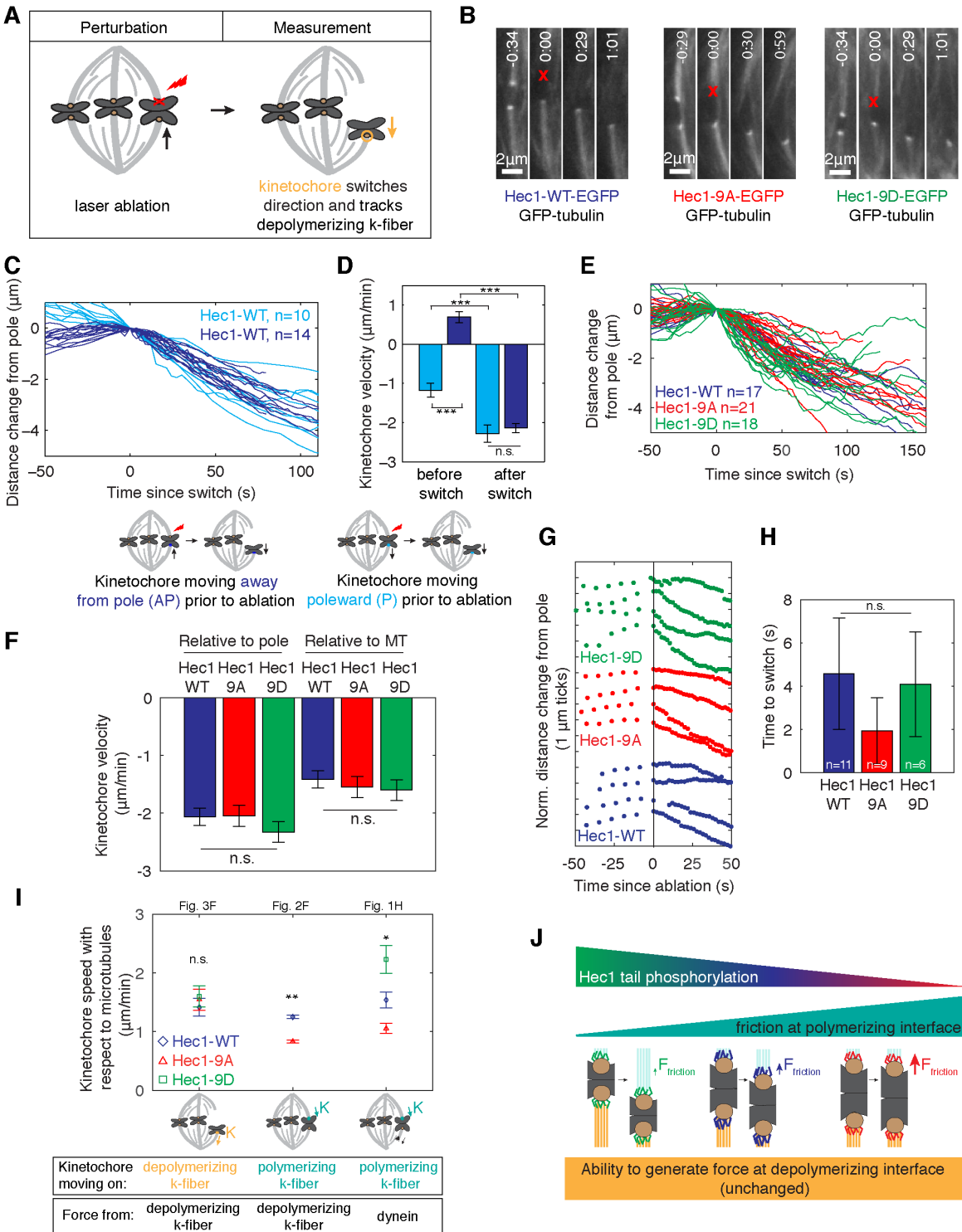


Figure 2.3 Hec1 tail phosphorylation does not disrupt the mammalian kinetochore's ability to couple to depolymerizing microtubules.

- A)** Assay to decouple sister kinetochores using laser ablation (red X) of one sister kinetochore to probe the remaining sister's ability to track depolymerizing microtubules.
- B)** Timelapse of Hec1-WT-EGFP, Hec1-9A-EGFP, or Hec1-9D-EGFP and GFP-tubulin in PtK2 cells before and after kinetochore ablation.
- C)** Response of kinetochores to sister ablation, colored by pre-ablation direction (n= number of kinetochores).
- D)** Kinetochore velocity relative to pole before and after its direction switch following sister ablation. (***) for $p < 0.001$, Student's T-test, n.s. for not significant).
- E)** Responses of kinetochores to sister ablation (n = number of kinetochores).
- F)** Kinetochore velocity after switching to poleward motion (depolymerization) due to ablation of sister. Kinetochore velocities relative to the pole (left) or to the microtubule lattice (right, adjusted for differences in flux from Fig. 2.2) (same dataset as (D), n.s. for not significant, Student's T-test).
- G)** Example traces and **(H)** mean delay of kinetochores switching direction after sister ablation (n.s. for not significant, Student's T-test).
- I)** Summary of the role of Hec1 phosphorylation in regulating kinetochore velocity under different mechanical states. Kinetochore speeds are replotted from the indicated figures (Fig. 2.1H values are adjusted for differences in flux from Fig. 2.2).
- J)** Cartoon summarizing the mechanical role of Hec1 tail phosphorylation: it regulates velocity in polymerization (top, cyan) but does not disrupt coupling in depolymerization (bottom, yellow). For simplicity, numbers of microtubules and Hec1 molecules are diagrammed as constant across conditions.

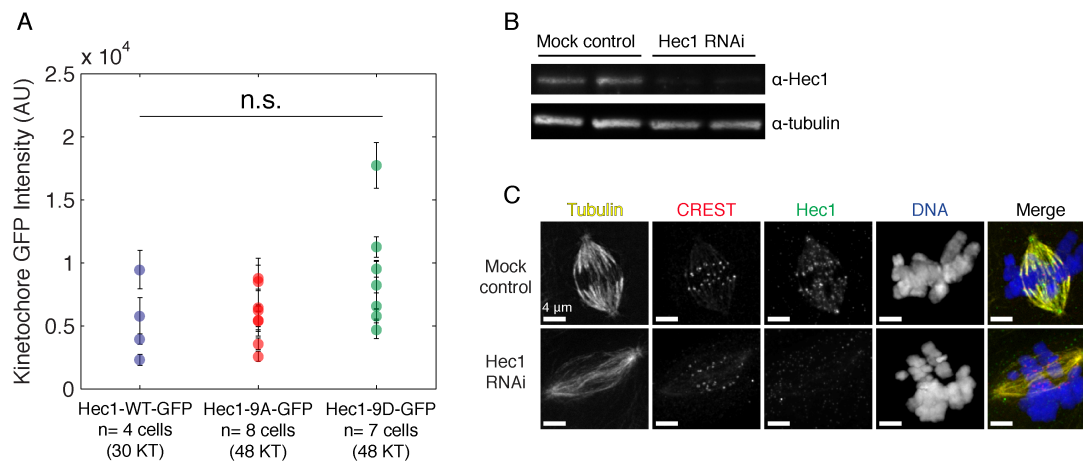


Figure S2.1 Validation of Hec1 depletion and rescue, related to Figure 2.1

A) Quantification of Hec1-GFP intensity in live cells. Cells measured here correspond to those analyzed in Figure 1. Each circle shows the mean and standard deviation for the fluorescence intensity of kinetochores measured in each cell for a 10x10-pixel box around kinetochores in focus in an individual cell in the 10 frames before laser ablation. Data represent average kinetochore intensity (4-8 kinetochores per cell) for the number of cells indicated per condition (n.s. not significant by Student's T test)

B) Immunoblot of mock-transfected and Hec1 siRNA-transfected PtK2 cell lysates stained for Hec1 and tubulin showing knockdown of endogenous Hec1 in PtK2 cells by RNAi (two replicates shown). **C.** Immunofluorescence images of mock-transfected and Hec1 siRNA-transfected PtK2 cells, stained with antibodies to Hec1. Chromosomes are stained with Hoechst, microtubules stained with antibodies against tubulin, and kinetochores labeled with anti-centromere antibodies (CREST).

Table 2.1 Role of Hec1 tail phosphorylation in regulating the mechanics of the mammalian kinetochore-microtubule interface

Data are presented as mean±SEM. See also Figures 2.1-3. n.a. for not applicable. n.s. for not significant.

^a $p < 0.05$ used as threshold for statistical significance using two tailed Student's T-Test. The abbreviations in the T-test column indicate which of the condition pairs are significantly different (e.g. WT,9D * indicates a significant difference between Hec1-WT and Hec1-9D).

^b There is no meaningful maximum K-K distance after ablation for Hec1-9D due to the variability of traces and lack of overshoot above baseline K-K distance from before ablation.

^c We made these calculations only on the subset of the data collected using photoactivation (Hec1-WT, n=42 and Hec1-9A n=34 kinetochores) since it allowed longer tracking of oscillations. We did not measure kinetochore velocities in Hec1-9D spindles since we were not able to track photomarks for long enough of the kinetochore oscillation cycle.

^d To adjust velocities to be relative to the microtubule lattice, we assumed poleward flux was unchanged from metaphase measurements (Fig. 2.2).

Table 2.1

Assay	Measurement	Experimental Condition			T-test ^a
		Hec1-WT	Hec1-9A	Hec1-9D	
K-fiber ablation (Fig. 1) [back kinetochore reflects passive interface]	Number of kinetochores (cells)	13 (4)	17 (8)	10 (7)	
	K-K distance before ablation (μm)	2.0 ± 0.1	2.5 ± 0.1	1.4 ± 0.1	WT,9A* WT,9D* 9A,9D*
	Time at max K-K distance after ablation (s)	95 ± 7	47 ± 5	n.a. ^b	WT,9A*
	Front kinetochore speed during poleward movement ($\mu\text{m}/\text{min}$)	1.7 ± 0.3	1.6 ± 0.2	1.8 ± 0.2	n.s.
	Distance back kinetochore moves during first 30 s of dynein pulling (μm)	0.7 ± 0.1	0.4 ± 0.1	1.0 ± 0.2	WT,9A* 9A,9D*
	Back kinetochore speed during poleward movement ($\mu\text{m}/\text{min}$)	0.9 ± 0.1	0.6 ± 0.1	1.7 ± 0.4	WT,9A* WT,9D* 9D,9A*
Metaphase spindle photomarking (Fig. 2.2) [passive interface]	Number of kinetochores (cells)	57 (29)	60 (24)	27 (8)	
	Poleward microtubule flux ($\mu\text{m}/\text{min}$)	0.65 ± 0.05	0.50 ± 0.03	0.73 ± 0.07	WT,9A* 9D,9A*
	Kinetochore velocity with respect to microtubule lattice ($\mu\text{m}/\text{min}$)	0.76 ± 0.04^c	0.51 ± 0.03^c	n.a. ^c	WT,9A*
	Kinetochore velocity > 0 (towards plus-end) with respect to microtubule lattice ($\mu\text{m}/\text{min}$)	1.25 ± 0.03^c	0.83 ± 0.03^c	n.a. ^c	WT,9A*
Kinetochore ablation (Fig. 2.3) [active + passive interface]	Number of kinetochores (cells)	17 (14)	21 (12)	18 (13)	
	K-K distance before ablation (μm)	2.3 ± 0.1	2.6 ± 0.1	1.7 ± 0.1	WT,9A* WT,9D* 9A,9D*
	Poleward kinetochore velocity after sister ablation ($\mu\text{m}/\text{min}$)	2.0 ± 0.2	2.1 ± 0.2	2.3 ± 0.2	n.s.
	Poleward kinetochore velocity relative to microtubule lattice after sister ablation ($\mu\text{m}/\text{min}$) ^d	1.5 ± 0.2	1.4 ± 0.2	1.6 ± 0.2	n.s.
	Time between front sister ablation and back kinetochore switch (s)	5 ± 3	2 ± 2	4 ± 2	n.s.

MATERIALS AND METHODS

Contact for Reagent and Resource Sharing

Further information and requests for resources and reagents should be directed to and will be fulfilled by the Lead Contact, Sophie Dumont (sophie.dumont@ucsf.edu).

Experimental Model and Subject Details

PtK2 cells (gift from T. Mitchison, Harvard University) were cultured in MEM (Invitrogen) supplemented with sodium pyruvate (Invitrogen), nonessential amino acids (Invitrogen), penicillin/streptomycin, and 10% qualified and heat-inactivated fetal bovine serum (Invitrogen) and maintained at 37°C and 5% CO₂.

Method Details

Cell culture and transfection of DNA and siRNA

For imaging, PtK2 cells were plated on glass-bottom 35mm dishes coated with poly-D-lysine (MatTek Corporation) and imaged in phenol red free MEM (Invitrogen) supplemented as above. PtK2 cells were transfected with WT-Hec1-EGFP, 9A-Hec1-EGFP, or 9D-Hec1-EGFP (human Hec1 phosphomutants in pEGFP-N1 vector; gifts from J. DeLuca, Colorado State University, CO) or pEGFP-tubulin (Clontech) or PA-

GFP-tubulin (gift A. Khodjakov, Wadsworth Center). siRNAs directed to PtK Hec1 (5'-AATGAGCCGAATCGTCTAATA-3') were purchased from Invitrogen or Sigma-Aldrich, and do not target human Hec1. Cells were transfected with DNA using FuGENE6 (Roche) or ViaFect (Promega) for 24 h before subsequent transfection with siRNA using Oligofectamine (Invitrogen) as described elsewhere (Guimaraes et al 2008). Cells were assayed 48 h after siRNA transfection. Control cells with Hec1 siRNA and no rescue construct robustly displayed phenotypes consistent with Hec1 knockdown (Fig. S2.1). Successful transfection and expression of Hec1 constructs was assessed by visualizing EGFP at kinetochores and, for mutants, by confirming that each cell examined had the expected K-K distance change. Cells expressing Hec1-9D-EGFP in a Hec1 RNAi background had widely varied spindle architecture and we included in our analysis cells that had visible EGFP expression and low K-K distance indicative of rescue but that still were able to form metaphase spindles and oscillate – which may include cells that still have a residual amount of endogenous Hec1 remaining. In Figure 2.1, 6/10 of the Hec1-9D-EGFP cells included tubulin labeled with 100nM SiR-tubulin dye (Spirochrome) and 10 μ M verapamil (Sigma-Aldrich) after incubation for 1h.

Immunofluorescence and immunoblotting

To validate knockdown (Fig. S2.1), mock control and siHec1 treated cells were fixed 48 h after siRNA transfection in 95% methanol with 5 mM EGTA for 3 min. The following antibodies and dyes were used: mouse Hec1-9G3 (1:1000, Novus), human anti-centromere protein (CREST, 1:25, Antibodies Inc.), rat anti-tubulin (1:500, AbD Serotec),

fluorescent secondary antibodies (1:500, Invitrogen), and Hoechst 33342 (1:1000, Sigma-Aldrich). For immunoblotting to validate knockdown, PtK2 cells were lysed 48 h after siRNA transfection. The following antibodies and dyes were used: mouse anti-tubulin DM1 α (1:5,000, Sigma) and anti-Hec1 9G3 (1:1,000, Novus), goat anti-mouse IgG-HRP (1:10,000, Santa Cruz Biotechnology, Inc.). Blots were exposed with SuperSignal West Pico Substrate (Thermo Scientific) and imaged with a Bio-Rad ChemiDoc XRS+ system.

Imaging and laser ablation

Live cells were imaged using a spinning disk confocal inverted microscope (Eclipse Ti-E; Nikon) described elsewhere [57] operated by MetaMorph (7.7.8.0; Molecular Devices). Cells were imaged with phase contrast (200-400ms exposure) and 488nm laser light (75-100ms exposure) through a 100x 1.45 Ph3 oil objective and 1.5x lens every 2-10s, in a stage-top incubation chamber (Tokai Hit) maintained at 30°C and 5% CO₂. Laser ablation (30-40 3-ns pulses at 20Hz) with 514 or 551nm light was performed using the MicroPoint Laser System (Photonic Instruments). For laser ablation experiments, images were acquired more slowly prior to ablation and then acquired more rapidly after ablation (typically 8s prior and 4s after ablation, except the latter was 2s for Fig. 2.3G). Successful k-fiber ablation was verified by loss of tension across the centromere (Fig. 2.1). Successful kinetochore ablation was verified by change in movement of the remaining sister kinetochore and depolymerization of the k-fiber associated with the ablated kinetochore (Fig. 2.3). Photomarking was performed using

the MicroPoint to deliver several pulses of either 514nm light to bleach GFP-tubulin (acquiring every 2-3s for at least 30s) or 405nm light to activate PA-GFP-tubulin (acquiring every 10s for at least 60s) (Fig. 2.2B,C). Fixed cells (Fig. S2.1 only) were imaged with exposure times of 5-200ms with DAPI, GFP, TRITC, and CY5 filter cubes and a mercury arc lamp on a Zeiss AxioPlan2 epifluorescence microscope (operated by MicroManager 1.4.13) with a 100x 1.4 DIC oil objective and a QIClick camera (QImaging).

Quantification and Statistical Analysis

Kinetochores, photomarks, ablation sites, and spindle poles were manually tracked from overlaid phase-contrast time-lapse and Hec1-EGFP (sometimes with GFP-tubulin or PA-GFP-tubulin) movies using a home-written MatLab (R2013b Version 8.2) program. Spindle poles were identified using the center of the GFP tubulin enriched region at the ends of the spindle. When no tubulin was co-transfected (Fig. 2.1), approximate spindle pole position was determined using phase contrast images (where the spindle can be identified since it excludes mitochondria). We manually selected the inflection points in kinetochore position as the start and end points of movement in one direction using plots of kinetochore position relative to the pole over time. We then calculated kinetochore velocity by fitting to a linear function (Fig. 2.1H-I; Fig. 2.3D,F; Table 2.1). We report (Fig. 2.1I) the distance traveled by kinetochores during the first 30 s after the start of dynein-induced poleward motion of a kinetochore pair, to avoid variability coming from differences in the duration of the poleward transport response. Poleward

microtubule flux (Fig. 2.2D) was calculated by measuring the position of the edge of the photomark closest to the kinetochore over time relative to the initial position (for PA-GFP-tubulin) for at least ~60s, or by measuring the position of the bleach mark over time relative to the pole (for GFP-tubulin) for as long as possible and in both cases performing a linear regression. Kinetochore velocity with respect to the microtubule lattice (k-fiber polymerization velocity) was calculated by measuring the distance between kinetochore and photomark on the same k-fiber for each pair of timepoints to get an instantaneous velocity that were pooled from different cells (Fig. 2.2E). Kinetochore velocities relative to the microtubule lattice after ablation were calculated by subtracting the mean value of poleward microtubule flux (Fig. 2.2B) from the measured velocity (Fig. 2.3F,I; Table 2.1). Time to kinetochore switching after ablation (Fig. 2.3H) was measured from the first frame after ablation to the frame when the kinetochore switched direction.

Data are reported as mean \pm SEM and for average traces (Fig. 2.1) data were collected into 8s wide bins before averaging. Sample sizes, statistical tests and p-values are indicated in the text, figures and figure legends. One-way ANOVA were performed using StatPlus (Version v6; AnalystSoft) and Two-tailed Student's T-tests were performed using MatLab.

ACKNOWLEDGEMENTS

We thank Jennifer DeLuca for Hec1-EGFP mutant constructs and advice, Ekaterina Grishchuk, Ted Salmon, Ron Vale, Dave Morgan, and David Agard for discussions, and

members of the Dumont Lab for discussions and critical reading of the manuscript. This work was funded by NIH DP2GM119177, NSF CAREER 1554139, the Rita Allen Foundation and Searle Scholars' Program (S.D.), and a NSF Graduate Research Fellowship (A.F.L.).

CHAPTER THREE

INDIVIDUAL KINETOCHORE-FIBERS LOCALLY DISSIPATE FORCE TO MAINTAIN ROBUST MAMMALIAN SPINDLE STRUCTURE

ABSTRACT

At cell division, the mammalian kinetochore binds many spindle microtubules that make up the kinetochore-fiber. To segregate chromosomes, the kinetochore-fiber must be dynamic and generate and respond to force. Yet, how it remodels under force remains poorly understood. Kinetochore-fibers cannot be reconstituted *in vitro*, and exerting controlled forces *in vivo* remains challenging. Here, we use microneedles to pull on mammalian kinetochore-fibers and probe how sustained force regulates their dynamics and structure. We show that force lengthens kinetochore-fibers by persistently favoring plus-end polymerization, not by increasing polymerization rate. We demonstrate that force suppresses depolymerization at both plus- and minus-ends, rather than sliding microtubules within the kinetochore-fiber. Finally, we observe kinetochore-fibers break but not detach from kinetochores or poles. Together, this work suggests an engineering principle for spindle structural homeostasis: different physical mechanisms of local force dissipation by the k-fiber limit force transmission to preserve robust spindle structure. These findings may inform how other dynamic, force-generating cellular machines achieve mechanical robustness.

INTRODUCTION

The spindle segregates chromosomes at cell division, and must do so accurately and robustly for proper cell and tissue function. In mammalian spindles, bundles of 15-25 microtubules called kinetochore-fibers (k-fibers) span from the kinetochore at their plus-

ends to the spindle pole at their minus-ends [3,77,78]. K-fibers are dynamic at both ends [59,79], and we now have a wealth of information on the molecular regulation of their dynamics [7,38,50]. To move chromosomes, k-fibers generate force through plus-end depolymerization [22,80,81]. Yet, while we are beginning to understand how the mammalian k-fiber generates force [35,46], we know much less about how force from the k-fiber and surrounding spindle in turn affects k-fiber structure and dynamics. Defining this relationship between k-fibers and their mechanical environment is central to understanding spindle structural homeostasis and function.

Force affects microtubule dynamics and structure in a variety of contexts [82]. From *in vitro* experiments coupling single microtubules to yeast kinetochore particles, we know that force can regulate all four parameters of microtubule dynamic instability [40,72]: it increases polymerization rates while slowing depolymerization, and favors rescue over catastrophe. From *in vivo* experiments, we know that force exerted by the cell correlates with changes in k-fiber dynamics [25,34,48,83,84], and that reducing and increasing force can bias k-fiber dynamics in different systems [47,61,64,65]. However, the feedback between force, structure and dynamics in the mammalian k-fiber remains poorly understood. For example, we do not know which dynamic instability parameters are regulated by force, or at which microtubule end. Similarly, we do not know how microtubules within the k-fiber remodel their structure (e.g. slide or break) under force, or the physical limits of the connections between k-fibers and the spindle. These questions are at the heart of understanding how the spindle can maintain its structure given its dynamic, force-generating parts [85,86]. Addressing these questions requires the ability to apply force on k-fibers with spatial and temporal control, while concurrently

imaging their dynamics. Yet, exerting controlled forces in dividing mammalian cells remains a challenge, and mammalian spindles and k-fibers cannot currently be reconstituted *in vitro*. Chemical and genetic perturbations can change forces on k-fibers *in vivo*, but these alter microtubule structure or dynamics, either directly or indirectly through regulatory proteins [87–89]. Thus, direct mechanical approaches are needed inside mammalian cells.

Here, we use glass microneedles to directly exert force on individual k-fibers inside mammalian cells and determine how their structure and dynamics remodel under sustained force. Inspired by experiments in insect spermatocytes [64,90,91], we sought to adapt microneedle manipulation to pull on k-fibers in mitotic mammalian cells for many minutes while monitoring their dynamics with fluorescence imaging. We show that forces applied for minutes regulate k-fiber dynamics at both ends, causing k-fiber lengthening, but do not cause sliding of the microtubules within them. Further, we demonstrate that sustained forces can break k-fibers rather than detach them from kinetochores or poles. Thus, k-fibers respond as a coordinated mechanical unit – remodeling at different sites to locally dissipate force, while preserving the connections between chromosomes and the spindle. Together, these findings suggest local force dissipation as an engineering principle for the dynamic spindle to maintain its structure and function under force and for other cellular machines to do the same.

RESULTS

Microneedle manipulation of mammalian spindles enables sustained force application on k-fibers with spatial and temporal control

To determine how mammalian k-fibers remodel under force, we sought an approach to apply forces with spatial and temporal control for sustained periods, compatible with cell health and live imaging of structure and dynamics. We adapted microneedle manipulation to pull on individual k-fibers in mammalian cells (Fig. 3.1A) and developed methods to do so gently enough to exert force for several minutes [92]. We used PtK cells as these are large and flat, have few chromosomes which allows us to pull on individual k-fibers, and are molecularly tractable [93]. We used a micromanipulator and a fluorescently labeled glass microneedle to contact a target metaphase PtK cell. We used microneedles with a diameter of $1.2 \pm 0.1 \mu\text{m}$ in the z-plane of the k-fiber. Pulling on an outermost k-fiber in the spindle for several minutes, we could reproducibly exert controlled forces, moving the microneedle with specific velocities over any given duration (Fig. 3.1B) and direction. The microneedle only locally deformed the cell membrane and spindle and remained outside of the cell, allowing precise, local control of where force is applied (Fig. 3.1C) [92]. Upon careful removal of the microneedle, cells could enter anaphase (Fig. 3.1D). These observations are consistent with cell health maintenance during these sustained manipulations. Thus, we can use microneedle manipulation to exert forces with spatial and temporal control over minutes on a

mammalian k-fiber, and thereby probe how force regulates k-fiber structure and dynamics.

Individual mammalian k-fibers switch to persistent lengthening in response to sustained applied force

To probe the response of k-fibers to force, we placed the microneedle along the k-fiber, within a few microns of the outermost sister kinetochore pair (Fig. 3.2A,B). We moved the microneedle at a speed of $5.2 \pm 0.2 \mu\text{m}/\text{min}$ for $3.1 \pm 0.3 \text{ min}$ (Fig. 3.1B), perpendicular to the spindle's long axis at the start of manipulation. We predicted that in response to force from the microneedle the spindle would either locally or globally deform (Fig. 3.2A). In response to this perturbation, the spindle translated and rotated, with faster microneedle speeds giving rise to faster spindle speeds (Fig. 3.2C,D). Thus we see global movement of the spindle in response to force. Yet, in these same spindles we also observed that k-fibers lengthened, indicating that the spindle also locally responds to force (Fig. 3.2E). During the pull, the manipulated k-fiber bent and lengthened by $4.1 \pm 0.8 \mu\text{m}$; meanwhile, an unmanipulated k-fiber in the same spindle half lengthened significantly less over the same duration (net k-fiber growth $0.03 \pm 0.32 \mu\text{m}$, Mann-Whitney U test, $p = 6 \times 10^{-5}$, Fig. 3.2F). Thus, force is dissipated locally by k-fiber bending and lengthening, and globally by whole spindle movements.

The manipulated k-fiber grew at $1.6 \pm 0.3 \mu\text{m}/\text{min}$, which was not significantly faster than its neighboring unmanipulated k-fiber during the growth phases of its oscillations ($1.4 \pm 0.1 \mu\text{m}/\text{min}$, Mann-Whitney U test, $p = 0.98$, Fig. 3.2G). However, the

manipulated k-fiber persistently lengthened (Fig. 3.2E), with either undetectable or very transient shortening, for longer than typical metaphase oscillations [48,94]. There was no correlation between k-fiber growth rate and pulling speed (Fig. 3.2H), suggesting either that force was dissipated before reaching the k-fiber's ends or that force does not regulate its maximum growth rate [21,36,65,95]. Further, the k-fiber growth rate did not vary with the proximity of the microneedle to the plus-end (Spearman R coefficient = 0.08, $p = 0.76$, Fig. 3.2I), which we hypothesized would lead to more direct force transmission, consistent with force not regulating the k-fiber's maximum growth rate. Together, these findings indicate that individual k-fibers remodel under sustained force for minutes by persistently lengthening. They also suggest that force inhibits their normal switching dynamics rather than substantially increasing their growth rate, which may serve as a protective mechanism to limit the rate of spindle deformations and thereby preserve spindle structure.

Force on individual mammalian k-fibers suppresses depolymerization at both ends without altering plus-end polymerization rates or inducing microtubule sliding

Metaphase mammalian k-fibers typically depolymerize at their minus-ends, and switch between polymerizing and depolymerizing at their plus-ends. Thus, force could lengthen k-fibers by increasing plus-end polymerization rates, by suppressing depolymerization at either end, by sliding microtubules within the k-fiber (Fig. 3.3A), or by a combination of these. To determine the physical mechanism of k-fiber lengthening under sustained force, we photomarked PA-GFP-tubulin on a k-fiber before micromanipulation and

tracked the photomark's position and size within the k-fiber (co-labeled with SiR-tubulin) (Fig. 3.3B) over time. In unmanipulated cells, photomarks fluxed towards the pole at a constant rate that reports on depolymerization at the minus-end (Fig. 3.3C) [59]. Upon external force from the microneedle, the photomark to pole distance remained constant (Fig. 3.3D), while the photomark to plus-end distance increased (Fig. 3.3E). This response indicates that applied force suppresses microtubule depolymerization at k-fiber minus-ends and that k-fibers lengthen by sustained polymerization at plus-ends.

Mapping these findings to the previous experiment measuring k-fiber lengthening (Fig. 3.2E,G), in the subset of k-fibers that lengthened (15/18), the growth rate was $1.9 \pm 0.4 \mu\text{m}/\text{min}$, which is the rate of plus-end polymerization given that depolymerization at both ends is inhibited (Fig. 3.3D,E). This is similar to the plus-end polymerization rate of neighboring unmanipulated k-fibers during natural growth: lengthening at $1.4 \pm 0.1 \mu\text{m}/\text{min}$ (Fig. 3.2G) while depolymerizing at the minus-end at $\sim 0.5 \mu\text{m}/\text{min}$ results in a polymerization rate of $\sim 1.9 \mu\text{m}/\text{min}$ at plus-ends (Mann-Whitney U test, $p = 0.55$) [33]. This indicates that the applied force does not increase mammalian k-fiber plus-end polymerization rates.

Notably, the average width of the photomark remained constant during manipulation (Fig. 3.3F,G), indicating the microtubules do not detectably slide within the bundle. Thus, the k-fiber behaves as a single coordinated mechanical unit, rather than as microtubules that independently respond to force. Together, our findings indicate that individual k-fibers lengthen under force by remodeling their ends, and not their bundle structure: force suppresses depolymerization locally at both plus- and minus-ends (Fig. 3.3), leads to persistent plus-end polymerization at a force-independent rate (Fig. 3.2,

3.3), and does so with the k-fiber responding as a single mechanical unit (Fig. 3.3). Thus, force is dissipated locally at k-fiber ends. This may limit force transmission to the rest of the spindle, thereby preserving overall k-fiber and spindle architecture for proper chromosome segregation.

The interfaces between mammalian k-fibers and the kinetochore and pole are more robust than k-fiber bundles under sustained force

Finally, we asked how k-fiber structure and spindle connections changed over the ~5-7 min lifetime of its microtubules [96–98], since this could set a timescale for their response to force. We hypothesized that as microtubules turn over the manipulated k-fiber could, for example, detach from the spindle or break (Fig. 3.4A). We used microneedles to pull on k-fibers for several minutes. Over these sustained pulls, we never observed k-fiber detachment from the kinetochore or pole, indicating strong anchorage at those force-dissipating sites [64,99–102]. Instead, k-fibers bent, lengthened, and then occasionally broke, 3.7 ± 0.5 min after the start of pulling (Fig. 3.4B). To probe the mechanism of this breakage, we examined k-fiber structure over time and the kinetics of breakage. K-fibers that broke sustained high curvature for many minutes before breaking (Fig. 3.4C), and reached a maximum curvature similar to those that did not ($p = 0.25$ Mann-Whitney U test, Fig. 3.4D). Further, k-fiber breakage kinetics appeared independent of the specific manner in which forces are exerted on the k-fiber: the time to breakage was similar when we moved the microneedle for a shorter time and held it in place, or pulled continuously for the entire duration of manipulation (Fig.

3.1B, 3.4E). Together, these suggested that the breakage process occurred gradually over sustained force, rather than rapidly by reaching an acute mechanical limit of k-fiber bending [103–106]. A k-fiber damage process that is gradual would promote breakage in response to sustained but not transient forces, setting a limiting timescale for restoring spindle structural homeostasis.

A possible model for gradual damage of the k-fiber over minutes is loss of microtubules as they turn over and fail to replenish within the k-fiber. In addition to turnover, it is also possible that there are alterations to k-fiber microtubule structure that would lead to gradual damage. During these manipulations, we observe microtubule plus-ends that appear to ‘splay’ from the bundle near the needle in 80% of k-fibers before breakage (Fig 3.4B,F), and when we can track plus-ends after breakage, they fail to depolymerize (Fig 3.4G). This is in contrast to abruptly created k-fiber plus-ends which depolymerize within seconds [57,58,107] and suggests a change in local microtubule structure prior to breakage that stabilizes plus-ends at the breakage site [106,108–111]. Together, these findings show how mammalian k-fibers gradually respond to and dissipate sustained forces over their microtubule’s lifetime. They robustly remain attached at kinetochores, yet eventually they locally break in the middle of the bundle, thereby preserving connections of chromosomes to the spindle at the expense of non-essential direct connections to poles [57,58].

DISCUSSION

In mammals, chromosome segregation is powered by dynamic k-fibers that both generate and respond to force. Here, we use microneedle manipulation to directly probe how k-fiber dynamics and structure respond to sustained force (Fig. 3.1). We thereby define how the spindle's longest-lived microtubule structure [96–98] remodels under force, which is key for understanding spindle structural homeostasis. We find that individual k-fibers respond to and dissipate sustained force by locally turning off microtubule depolymerization at both plus- and minus-ends (Fig. 3.2, 3.3), and eventually breaking on the timescale of their microtubule turnover (Fig. 3.4). They do so without increasing their rate of plus-end polymerization (Fig. 3.2, 3.3), without sliding their microtubules within the k-fiber (Fig. 3.2, 3.3) and without detaching from kinetochores or poles (Fig. 3.4). Thus, how the k-fiber responds – and doesn't respond – to force allows it to act as a single mechanical unit that can maintain its connections to chromosomes and preserve global spindle structure. The ability to directly exert force on the mammalian spindle is key to this work as it allowed us to clearly probe the feedback between force, structure, and dynamics in the spindle [86]. Together, these findings suggest different physical mechanisms of local force dissipation as an engineering principle for the spindle to maintain its structure and function under sustained forces (Fig. 3.5). More broadly, this study provides a framework for understanding how the spindle remodels under force during chromosome segregation.

We show that mammalian k-fiber plus-ends persistently polymerize at normal rates in response to applied force (Fig. 3.2, 3.3). In contrast, microtubules attached to yeast kinetochore particles or subcomplexes *in vitro* polymerize faster at higher force, in

addition to suppressing catastrophe and favoring rescue under force [40,112]. In newt cells, force induces persistent k-fiber lengthening at normal k-fiber growth rates [65], and our findings suggest that this may occur through regulation of dynamics at both ends. The different force-velocity relationships at kinetochore-microtubule plus-ends in mammals and yeast kinetochore particles could, for example, stem from differences in applied forces, kinetochore architecture [113], or additional regulation in cells. The molecular basis of potential “governors” of k-fiber plus-end polymerization velocity has been a long standing question [21,33,36], and our findings suggest that in mammals this molecular “governor” is not mechanically regulated. Notably, force not regulating mammalian k-fiber polymerization velocity (Fig. 3.2, 3.3) could provide a protective upper limit to how fast the spindle can remodel. It also has implications for mechanical communication in the spindle, for example how force regulates kinetochore-microtubule attachments [52,114].

We demonstrate that force not only regulates the dynamics of individual k-fibers’ plus-ends, but also of their minus-ends (Fig. 3.3). Thus, both k-fiber ends serve as sites of force dissipation, allowing forces exerted on k-fibers to be locally and robustly dissipated, thereby limiting disruption to the rest of the spindle. The fact that force regulates minus-end dynamics of single k-fibers indicates that their regulation occurs at the level of the individual k-fiber, and not globally as hypothesized when force was applied to the whole spindle [115,116]. Though we cannot exclude it, we did not detect force-induced polymerization at k-fiber minus-ends, and thus force dissipation also appears limited at minus-ends. The microneedle approach we present here, combined with perturbations of microtubule regulators at minus-ends [44,117], will be key in

defining the molecular basis of the regulation of k-fiber minus-end dynamics by force. Together, the response of individual k-fibers' dynamics to force, at both ends, allows each k-fiber to locally isolate and dissipate applied force while retaining its internal organization and global spindle structure. Therefore k-fiber end dynamics mechanically buffer global spindle deformations from local forces to maintain structural homeostasis [42,43].

On longer timescales, we find that the k-fiber breaks under force, without detaching from the kinetochore or pole (Fig. 3.4). This is surprising as force-induced detachments from kinetochores occur *in vitro* [40] and in meiotic insect cells [91,118–120]. This difference could, for example, arise from variations in force application, or in the physical properties or architectures of their kinetochores [16,25,26,28]. Instead of detaching, the k-fiber breaks on a timescale similar to that of its microtubule lifetime, suggesting that the k-fiber's lifetime may limit the long-term impact force can have over spindle structure. Our findings suggest a model of gradual k-fiber damage, and that sustained force may not only regulate biochemistry at the k-fiber's ends, but also in its middle along the microtubule lattice (Fig. 3.4F,G). Local defects in the lattice can replenish GTP-tubulin, creating stable sites for microtubule repair or enzymatic activities that may alter the physical properties of microtubules [106,108–111]. Under sustained force, k-fiber attachments to chromosomes are prioritized over direct connections between chromosomes and poles, which are not necessary for segregation [57,58] and thus may not be key for function.

Altogether, we show that mammalian spindles locally dissipate sustained force by remodeling k-fiber dynamics and structure through different physical mechanisms

over time (Fig. 3.5). In principle, this can allow the spindle to preserve robust connections to chromosomes, and maintain its structure under force throughout mitosis. Local dissipation of force limits its impact on the rest of the spindle, providing local isolation. In turn, the timescale of such dissipation limits the timescale of mechanical memory in the spindle. By regulating force dissipation, the spindle could set the impact force has on its structure over time to allow it to respond to different mechanical cues and perform different mechanical functions. Looking forward, it will be of interest to map how spindles with different k-fiber dynamics and structures across species dissipate and transmit force, and thereby preserve their structural homeostasis [64,121–124]. Finally, we note that the local force dissipation at multiple sites we observe in the spindle is a simple engineering principle by which a cellular structure may be mechanically robust, analogous to how structural engineers design sites of local force dissipation to make buildings and bridges robust to external forces.

FIGURES AND FIGURE LEGENDS

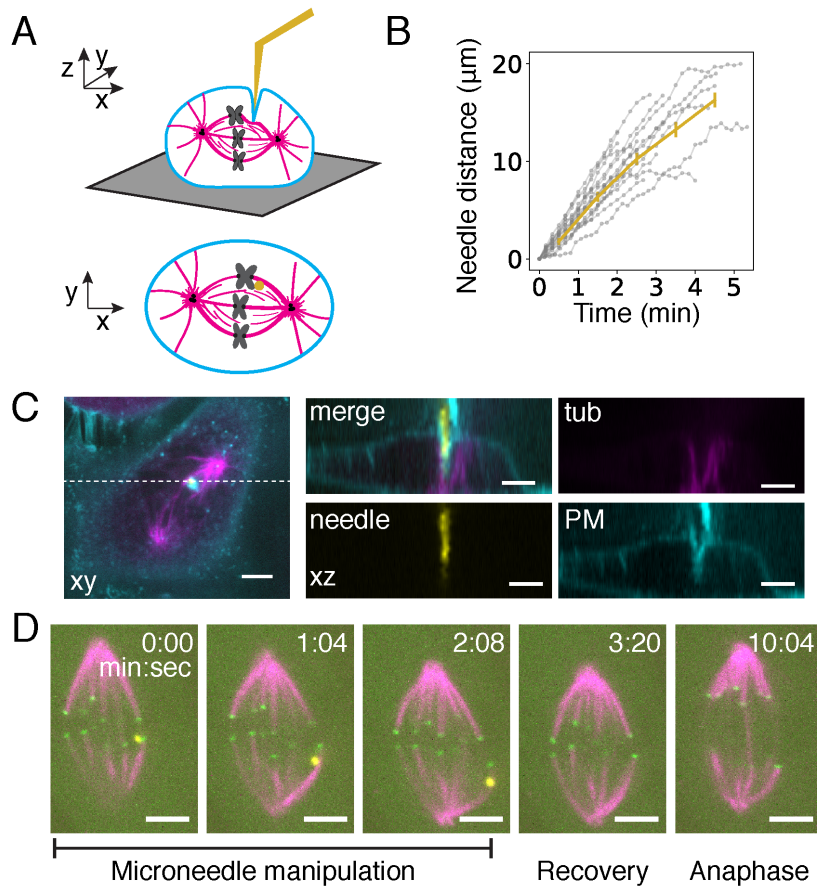


Figure 3.1. Microneedle manipulation of mammalian spindles enables sustained force application on k-fibers with spatial and temporal control.

A) Cartoon representation of microneedle (yellow) placement (3D and cross-section) in a metaphase mammalian cell to exert sustained force on a k-fiber.

B) Plot of linear microneedle displacement over time during manipulation in metaphase PtK cell (mean \pm SEM, $n = 18$ cells). This approach allows smooth, reproducible pulls on single mammalian k-fibers.

C) Representative z-stack reconstruction shows geometry of microneedle contact with the cell and metaphase spindle (GFP-tubulin, magenta) as diagrammed in **(A)**. The plasma membrane (CellMask Orange dye, cyan) locally deforms around the microneedle (Alexa-647, yellow) but does not alter whole cell shape or puncture the cell. Scale bar = 4 μm .

D) Representative timelapse images of microneedle (Alexa-555, yellow) manipulation to exert force on a k-fiber: it displaces the metaphase spindle (Cdc20-YFP, green; SiR-tubulin, magenta) and deforms the pulled k-fiber. Manipulated spindles typically progress to anaphase (here at 10:04). Scale bar = 4 μm .

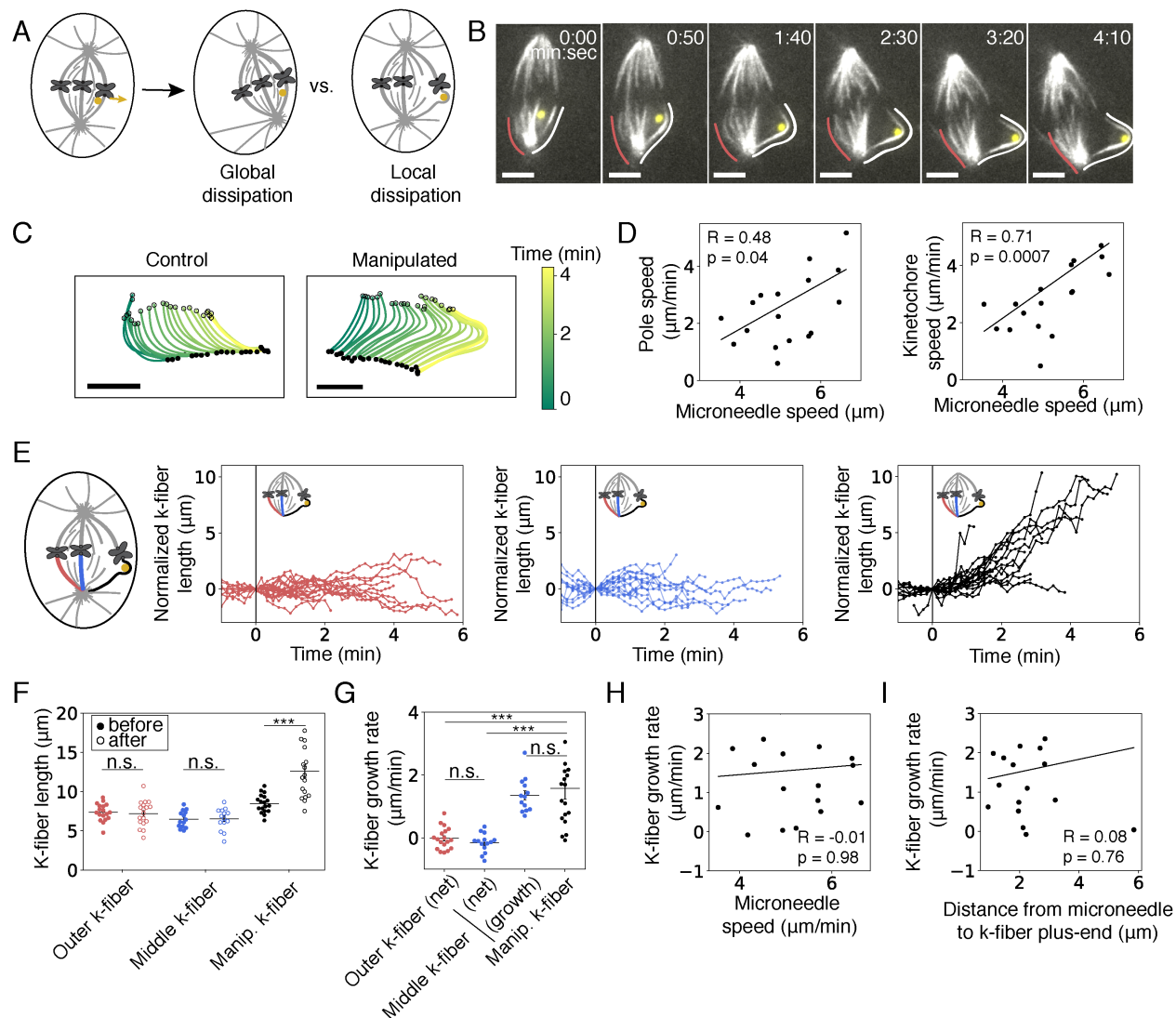


Figure 3.2. Individual mammalian k-fibers switch to persistent lengthening in response to sustained applied force.

A) Assay to locally exert force on an outer k-fiber using a microneedle (yellow circle) to probe its response to force (yellow arrow). Possible outcomes include global movement of the whole spindle and local deformation of the k-fiber, reflecting global and local dissipation of applied force, respectively.

B) Representative timelapse images of spindle and k-fiber (SiR-tubulin, white) movement and remodeling in response to sustained force from a microneedle (Alexa-555, yellow) as in Fig. 3.1B. The whole spindle rotates and translates while the k-fiber proximal to the microneedle (white line, tracked) bends and lengthens compared to a control k-fiber (red line, tracked). Scale bar = 4 μm .

C) Maps of the tracked k-fiber shapes and positions for control and manipulated k-fibers from **(B)**. Open circles indicate plus-end positions and filled circles indicate pole positions. The manipulated k-fiber (right) translates in the XY plane and bends and lengthens over time; the control k-fiber (left) similarly translates but does not lengthen.

D) Speed of proximal pole (left) and plus-end (kinetochore, right) movement relative to the speed of microneedle movement within a half-spindle. Half-spindle movement is positively correlated with microneedle speed, indicating global dissipation of force (pole: Spearman $R = 0.48$, $p = 0.04$; plus-end: Spearman $R = 0.72$, $p = 0.0007$, $n = 18$ cells).

E) K-fiber length as a function of time, normalized by subtracting the initial length at start of force application ($t = 0$) for k-fibers manipulated (right, black, $n = 18$ cells), in the middle of the half-spindle (middle, blue, $n = 13$ cells), and on the opposite side of the half-spindle (left, red, $n = 18$ cells). The micromanipulated k-fiber lengthens persistently during force application while the other k-fibers grow and shrink but don't systematically change length.

F) Average k-fiber lengths at start and end of force application as a function of k-fiber position in the half-spindle. The manipulated k-fiber (black, $n = 18$ cells) significantly increased in length ($p = 0.0002$, Wilcoxon signed-rank test) while the middle and outer k-fiber lengths remain unchanged ($p = 0.73$, $n = 13$ cells and $p = 0.35$, $n = 18$ cells, Wilcoxon signed-rank test). Plot shows mean \pm SEM.

G) Plot of average k-fiber growth rate for manipulated k-fibers (black, $n = 18$ cells) compared to middle k-fibers (blue, $n = 14$ cells) or outer k-fibers (red, $n = 18$ cells) in the same half-spindle. Only the manipulated k-fiber lengthened significantly during force application while neighboring k-fibers continued oscillating between lengthening and shortening phases (manipulated k-fiber versus middle k-fiber 'net', $p = 1.6 \times 10^{-5}$, manipulated k-fiber versus outer k-fiber 'net', $p = 1.4 \times 10^{-5}$, middle k-fiber 'net' compared to outer k-fiber, ($p = 0.3$, Mann-Whitney U test). The growth rate of the manipulated k-fiber was not significantly different than the growth rate of the middle k-fiber during just the growth phases of its oscillations (blue 'growth', $p = 0.98$, Mann-Whitney U test). Plot shows mean \pm SEM.

H) Growth rate of the manipulated k-fiber as a function of the speed of microneedle movement. The growth rate of the manipulated k-fiber did not correlate with the speed of microneedle movement (Spearman $R = 0.21$, $p = 0.46$, $n = 18$ cells).

I) Growth rate of the manipulated k-fiber as a function of distance between the microneedle center and the k-fiber plus-end. The growth rate of the manipulated k-fiber does not correlate with the proximity of the microneedle to the plus-end (Spearman $R = 0.04$, $p = 0.88$, $n = 18$ cells).

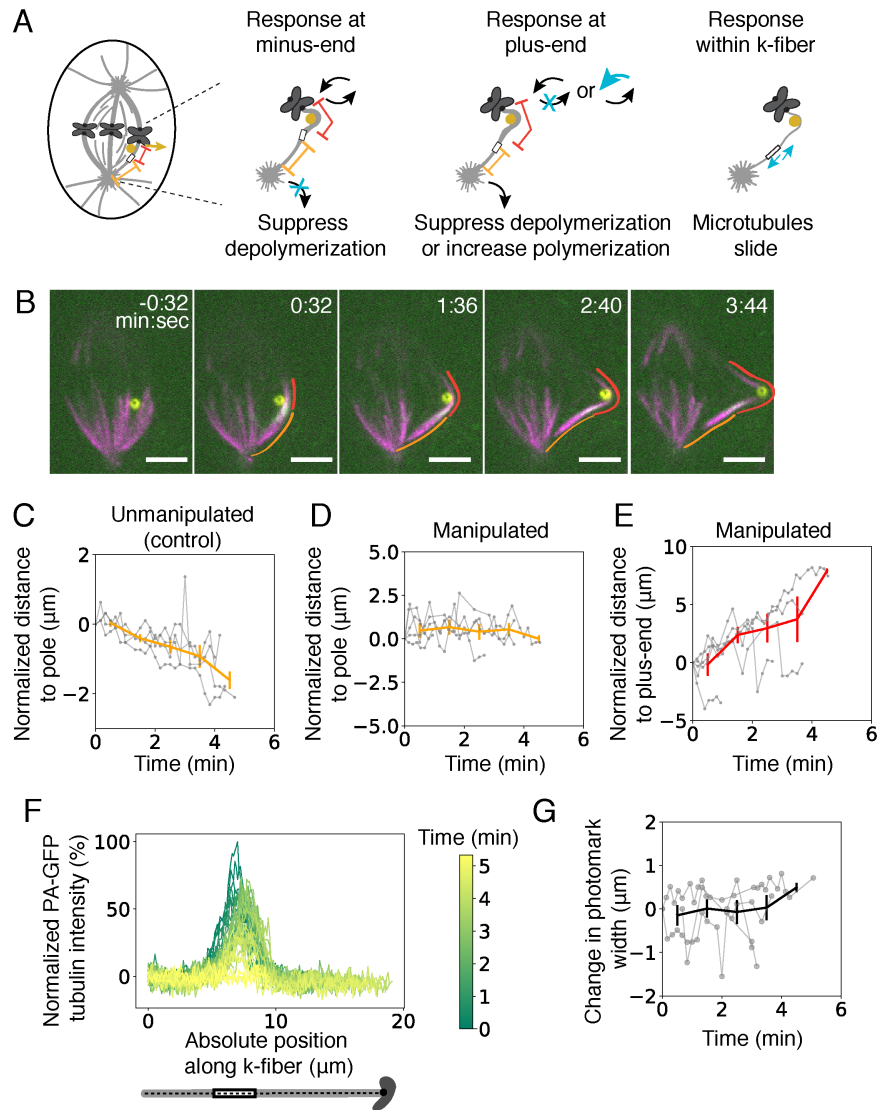


Figure 3.3. Force on individual mammalian k-fibers suppresses depolymerization at both ends without altering plus-end polymerization rates or inducing microtubule sliding.

A) Assay to determine the physical mechanism of k-fiber lengthening under force by tracking position of a photomark on the k-fiber during microneedle manipulation. Possible outcomes are shown, not mutually exclusive: the photomark could remain fixed relative to the pole indicating a suppression of minus-end depolymerization (left, blue 'X'), the position of the photomark to the kinetochore could increase continuously, indicating a suppression of plus-end depolymerization or increase in plus-end polymerization rate (middle, blue 'X' or arrow), or the photomark could remain in a fixed position but widen, indicating sliding of microtubules within the k-fiber (right, blue 'X').

B) Representative timelapse images of photomark (PA-GFP tubulin, white) during microneedle (Alexa-555, yellow) manipulation of a k-fiber (SiR-tubulin, magenta). The

distance between the photomark and the pole remains constant (orange line) while the distance between the photomark and plus-end increases (red line). Scale bar = 4 μm .

C) Plot of the photomark to the pole distance change over time due to flux of microtubules in unmanipulated cells, as a baseline (n = 4 cells).

D) Plot of the photomark to pole distance change during microneedle manipulation, showing that photomark movement poleward due to microtubule depolymerization is suppressed (n = 4 cells).

E) Plot of the photomark to plus-end position distance change during microneedle manipulation, showing that k-fibers persistently polymerize at their plus-ends under force (n = 4 cells).

F) Representative example of photomark intensity linescans over time during manipulation, from same cell as **(B)**.

G) Change in full-width at half-max photomark intensity at each timepoint during microneedle manipulation, showing that photomarks do not widen under force, and thus that there is no detectable microtubule sliding within the k-fiber (n = 4 cells).

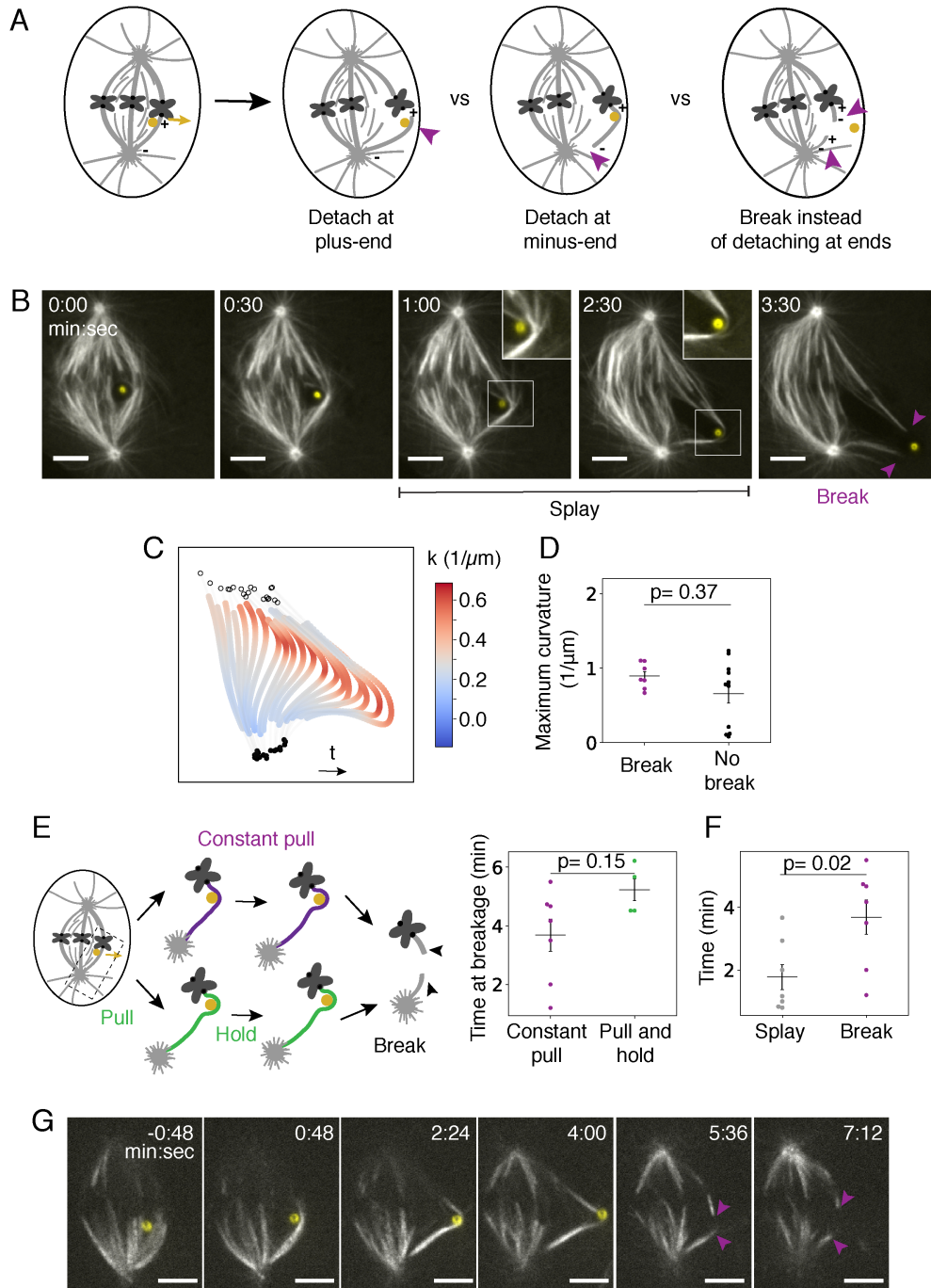


Figure 3.4. The interfaces between mammalian k-fibers and the kinetochore and pole are more robust than k-fiber bundles under sustained force.

A) Assay to probe how the k-fiber response to sustained force for minutes. Three example outcomes of force application (yellow arrow) are shown: the k-fiber could detach (purple arrow) from the kinetochore (left), the k-fiber could detach (purple arrow) from the pole (middle), or the k-fiber could remain attached at its ends but break (purple arrows) in its center (right).

B) Representative timelapse images of k-fiber (GFP-tubulin, white) bending, lengthening and breaking under sustained force. Before the k-fiber breaks, microtubules appear (insets) on the outside of the deformed k-fiber near the area of high curvature next to the microneedle (Alexa-647, yellow). The break creates new microtubule bundle plus-ends (purple arrowheads). Scale bar = 4 μm .

C) Example map of local curvature (k) along a k-fiber bundle during sustained microneedle manipulation. As the k-fiber bends over time, high curvature (dark red) increases near the microneedle and persists for many minutes before breakage occurs (3.5 min). Open circles indicate plus-end positions and filled circles indicate pole positions.

D) Maximum curvature along the k-fiber in the last tracked timepoint before breakage in cells with breakage events (purple, $n = 6$ cells) or at the end of the manipulation for cells with no breakage (black, $n = 11$ cells, plot shows mean \pm SEM, $p = 0.37$, Mann-Whitney U test).

E) Cartoon of two different micromanipulation assays that lead to k-fiber breakage: (top, purple) microneedle is moved continuously at $5.2 \pm 0.2 \mu\text{m}/\text{min}$ for 3.1 ± 0.3 minutes, (bottom, green) microneedle is moved at $4.5 \pm 0.7 \mu\text{m}/\text{min}$ for 1.7 ± 0.2 min and then held in place until breakage. Plot showing no significant difference in the time at breakage in each assay (plot shows mean \pm SEM, $n = 7$ cells and 4 cells, $p = 0.15$, Mann-Whitney U test).

F) Plot of the average time to a splaying event (where newly visible microtubules appear near the area of high curvature) and average time to breakage for the subset of cells in which both events occurred. Splaying events occurred significantly before breakage events (plot shows mean \pm SEM, $n = 9$ cells, $p = 0.007$, Wilcoxon signed-rank test).

G) Example timelapse images of breakage event in which the newly created bundle plus-ends (lower purple arrow) are highly stable and persist for minutes after breakage. This example cell is the same as shown in Fig. 3.3B but here displaying the full response including breakage.

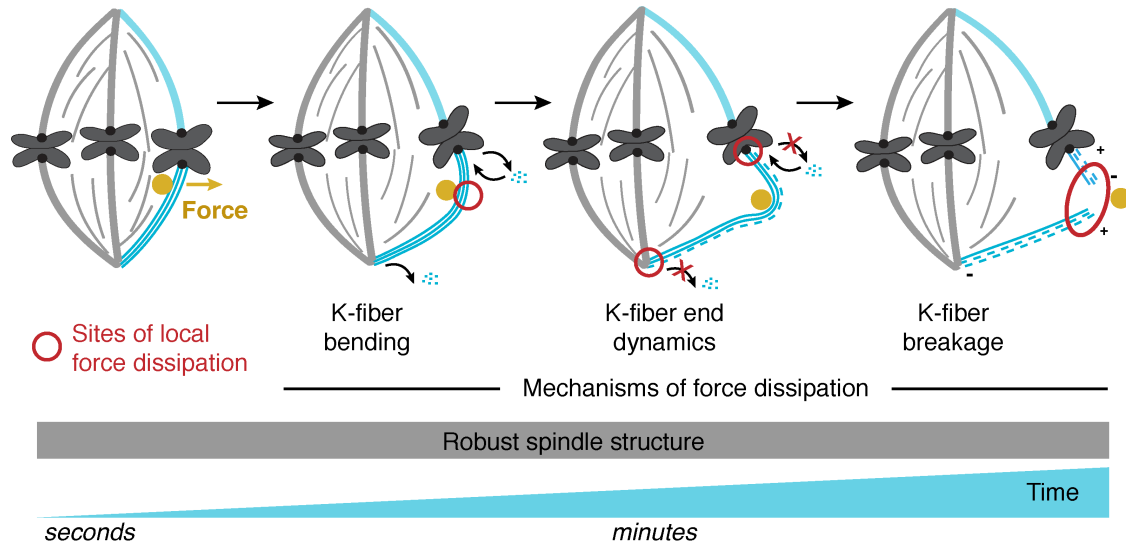


Figure 3.5. A model for local force dissipation by individual k-fibers to maintain robust mammalian spindle structure.

Using micromanipulation to apply sustained forces (yellow circle, arrow) on individual mammalian k-fibers reveals that they locally dissipate force (red circles) using different physical mechanisms over different timescales (blue ramp, dashed lines indicate microtubule turnover) to robustly preserve global spindle structure (gray box). Key to this model is how k-fibers both remodel under and resist sustained force. K-fibers *remodel* and locally dissipate force: they bend (second panel), lengthen through suppressing depolymerization at their plus- and minus-ends (third panel, small black 'off' arrows with red 'X'), and gradually break (fourth panel). In turn, k-fibers also *resist* force to preserve spindle structure: they do not increase their polymerization rate (small black 'on' arrows), slide their microtubules, or detach from kinetochores or poles under force. Note that for simplicity, we do not diagram whole spindle movements and only show individual microtubules for the manipulated k-fiber. Thus, local dissipation and isolation mechanisms together preserve mammalian spindle structure under sustained forces: the former limit how far and for how long forces can be transmitted across the spindle, while the latter limit the spindle's deformation rate and preserve k-fiber and spindle structure and their connections. Together, this model suggests local force dissipation at multiple sites as an engineering principle for the dynamic spindle and other cellular machines to robustly maintain their structure and function under force.

MATERIALS AND METHODS

Cell culture

PtK2 cells were cultured in MEM (Invitrogen) supplemented with sodium pyruvate (Invitrogen), nonessential amino acids (Invitrogen), penicillin/streptomycin, and 10% qualified and heat-inactivated fetal bovine serum (Invitrogen) and maintained at 37°C and 5% CO₂. PtK2 cells stably expressing human GFP- α -tubulin (gift from A. Khodjakov, Wadsworth Center) and PtK2 cells incubated with SiR-tubulin dye were both used. PtK2 cells stably expressing human EYFP-Cdc20 (gift from Jagesh Shah, Harvard Medical School) were used for Fig. 3.1 validation of microneedle manipulation. SiR-tubulin (Cytoskeleton, Inc.) at 100nM and 10 μ M verapamil (Cytoskeleton, Inc.) were incubated with cells for 45 min prior to imaging for cells not expressing GFP-tubulin. PtK1 cells stably expressing PA-GFP tubulin (gift from A. Khodjakov) were cultured in F12 media (Invitrogen) supplemented with penicillin/streptomycin, and 10% qualified and heat-inactivated fetal bovine serum (Invitrogen) and maintained at 37°C and 5% CO₂. For photoactivation experiments, PtK1 PA-GFP tubulin cells were co-labeled with SiR-tubulin as above to mark overall spindle structure. Control cells labeled with SiR-tubulin that did not undergo microneedle manipulation still exhibited chromosome oscillations and poleward microtubule flux at a rate of $0.40 \pm 0.06 \mu\text{m}/\text{min}$ (Fig. 3.3C), indicating that this concentration and length of dye incubation did not suppress k-fiber microtubule dynamics in these cells.

Microscopy

Live cells were imaged using an inverted microscope (Eclipse Ti-E; Nikon) with a spinning disk confocal (CSU-X1; Yokogawa Electric Corporation), head dichroic Semrock Di01-T405/488/568/647 for multicolor imaging, equipped with 405 nm (100 mW), 488 nm (120mW), 561 nm (150mW), and 642 nm (100mW) diode lasers, emission filters ET455/50M, ET525/ 50M, ET630/75M and ET690/50M for multicolor imaging, and an iXon3 camera (Andor Technology) operated by MetaMorph (7.7.8.0; Molecular Devices). Cells were imaged with a 100x 1.45 Ph3 oil objective and 1.5x lens every 10 s acquiring 3 z-planes spaced 0.35 – 0.50 μm apart with a PZ-2000 z-piezo stage (ASI). Cells were imaged in a stage-top incubation chamber (Tokai Hit) with the top lid removed and maintained at 30°C. Cells were plated on glass-bottom 35mm dishes coated with poly-D-lysine (MatTek Corporation) and imaged in CO₂ independent MEM (Invitrogen) supplemented as for PtK2 cell culture as described above.

Photoactivation was performed using a MicroPoint pulsed laser system (Andor) to deliver several 3-ns 20Hz pulses of 405nm light to activate PA-GFP-tubulin (Fig. 3.3).

Microneedle manipulation

Microneedle manipulation was adapted for use in mammalian spindles for sustained periods of many minutes by optimizing needle dimensions, contact geometry, and speed of motion to minimize cellular damage. Further microneedle manipulation details can be found in [92].

Preparation of microneedles:

Glass capillaries with an inner and outer diameter of 1 mm and 0.58 mm respectively (1B100-4 and 1B100F-4, World Precision Instruments) were used to create microneedles using a pipette puller (P-87, Sutter Instruments, Novato, CA). For a ramp value of 504 (specific to the type of glass capillary and micropipette puller), we used the following settings: Heat = 509, Pull = 70, velocity = 45, delay = 90, pressure = 200, prescribed to generate microneedles of 0.2 μm outer tip diameter (Sutter Instruments Pipette Cookbook). The measured diameter of the microneedle in the z-plane of the manipulated k-fiber was $1.2 \pm 0.1 \mu\text{m}$ (the tip was placed deeper than the k-fiber to ensure that it would not slip during movement). Microneedles with longer tapers and smaller tips than above were more likely to rupture the cell membrane. Microneedles were bent ~ 1.5 mm away from their tip at a 45° angle using a microforge (Narishige International, Amityville, NY). This allowed for microneedles placed in the manipulator at a 45° angle to approach the cell vertically and minimize the overall surface area of contact between the microneedle and the cell membrane.

Microneedles used for manipulation were coated with BSA Alexa Fluor 647 (A-34785, Invitrogen) or 555 conjugate (A-34786, Invitrogen) by soaking in the solution for 60 s before imaging [125]: BSA-Alexa-647 and Sodium Azide (Nacalai Tesque, Kyoto, Japan) were dissolved in 0.1 M phosphate-buffered saline at the final concentration of 0.02% and 3 mM, respectively. Tip labeling was critical towards improving cell health during sustained manipulations because it allowed us to better visualize the microneedle tip in fluorescence along with the spindle and prevented us from going too deeply into the cell, thereby causing rupture.

Selection of cells:

Cells for micromanipulation were chosen based on being at metaphase, being flat, with a spindle having two poles in the same focal plane. These criteria were important for pulling on single k-fibers close to the top of the cell and simultaneously being able to image the whole spindle's response over several minutes of manipulation. Cells were included in our datasets if they did not appear negatively affected by micromanipulation. We did not include cells that underwent sudden and continuous blebbing upon microneedle contact, cells with spindles that started to collapse during manipulation or cells with decondensed chromosomes.

Manipulation:

Manipulations were performed in 3D using an xyz stepper micromanipulator (MP-225 Sutter Instruments). A 3-knob controller (ROE-200, Sutter Instruments) connected to the manipulator and controller (MPC-200, Sutter Instruments) allowed fine manual movements and was used to find and position the microneedle before imaging. To find and position the microneedle, we first located and centered the microneedle tip in the field of view using a low magnification objective (20X 0.5NA Ph1 air). We placed the microneedle in focus just above the coverslip before switching to a 100X 1.45 Ph3 oil objective and refined the xyz position of the microneedle to be right above a cell of interest, using the Ph1 phase ring to confirm microneedle position (phase ring mismatch visually highlights the position of the glass microneedle).

Upon choosing a cell to manipulate, we identified an outer k-fiber in a plane close to the top of the cell focused on this k-fiber. Then, we slowly brought the microneedle down into the cell using the fluorescent label of the microneedle tip to inform on its position until just deeper than the k-fiber of interest. If the microneedle's position was too far away from the k-fiber of interest, we slowly moved the microneedle out of the cell, adjusted its xy position and brought it back down into the cell. Through this iterative process, we could correctly position the microneedle such that it was inside the spindle, next to the outer k-fiber.

Once the microneedle was positioned next to an outer k-fiber near the top of the cell, it was moved in a direction that is roughly perpendicular ($\sim 60^\circ$ - 90°) from the spindle's long axis using software (Multi-Link, Sutter Instruments). We wrote a custom program to take as inputs the desired angle, duration, and distance for the microneedle movement and then output a set of instructions in steps, x, y positions, and delays for the Multi-Link software to achieve to desired movement. For all manipulations except those in Fig. 3.4E, we moved the microneedle at $5.2 \pm 0.2 \mu\text{m}/\text{min}$ for $3.1 \pm 0.3 \text{ min}$ (Fig. 3.1B). For the 'pull and hold' experiments, we moved the microneedle at $4.5 \pm 0.7 \mu\text{m}/\text{min}$ for $1.7 \pm 0.2 \text{ min}$ and then held in place until breakage (Fig. 3.4E). At the end of the manipulation the microneedle was manually removed from the cell in the z-axis slowly ($<5 \mu\text{m}/\text{min}$) to avoid membrane rupture or cell detachment from the coverslip.

Tracking of spindle features

For all analyses (Fig. 3.2-4), k-fibers were manually tracked in Fiji (version 2.0.0-rc-68/1.52g) [126] by drawing segmented lines along maximum intensity projections of

three z planes of the fluorescent image with “spline fitting” checked. Splines were drawn from the edge of the tubulin signal at the plus-end to the center of the area of high tubulin intensity at the pole since we cannot determine specifically the location of the minus-end of the k-fiber. Spline x and y coordinates were saved in CSV files using a custom macro in Fiji and imported into Python. All subsequent analysis and plotting was performed in Python. Microneedle position was tracked using the mTrackJ plugin [127] in Fiji using the “snap to bright centroid” feature and coordinates were saved in CSV files and imported into Python for further analysis.

Quantification of spindle features

Pole and kinetochore position were calculated using the x and y coordinates of the point at the end of the spline that terminated at the pole and kinetochore, respectively. Time $t = 0$ was set to the first frame after the start of microneedle movement. Pole, microneedle, and kinetochore speed were calculated using the average displacement of the ends of the spline or center of the microneedle position over time (Fig. 3.2D,H). K-fiber length and net growth rate were calculated using the length of the spline over time and with linear regression from the start and end of the manipulation (Fig. 3.2E-I). For the analysis of k-fiber growth rate of unmanipulated k-fibers specifically during the growth phase (Fig. 3.2G), the start and end points were selected manually when there were at least three consecutive timepoints where the k-fiber length increased. The distance between the microneedle and plus-end was calculated as the linear distance between the center of the microneedle centroid and the plus-end terminus of the spline (Fig. 3.2I). Microtubule ‘splaying’ was manually scored as the first frame in which new

microtubule density appeared on the side of the k-fiber near the point of high curvature (Fig. 3.4B,F). These events occurred within one time point (<10s), thus their dynamics of appearance could not be carefully characterized under these imaging conditions. K-fiber breakage was manually scored as the first frame in which the two k-fiber pieces moved in an uncorrelated manner (Fig. 3.4B,E-G).

Photomark analysis

For photomark analysis, splines were tracked on maximum intensity projections of three z-planes using the 647 channel (SiR-tubulin label) and then that spline with a thickness of 5 pixels was used to calculate the intensity in the 488 channel (PA-GFP tubulin) at each point using a custom-written macro in Fiji, with all subsequent analysis in Python. Photomark position over time was calculated using the position along the curved k-fiber spline at which the maximum intensity value occurred after masking bright intensity directly at the pole that was separate from the photomark signal (Fig. 3.3C-E). Points were only included if the photomark remained in focus above background fluorescence. K-fiber intensity was normalized to the average intensity of the k-fiber in the timepoint prior to photomarking to identify the peak, however no intensity measurements were performed due to fluctuation of the k-fiber in the z-axis beyond the 3 z-planes measured. For calculation of photomark width (Fig. 3.3F), Gaussian fitting was performed on the normalized k-fiber intensities and the full-width at the half-maximal intensity (FWHM) was calculated using the width of the distribution (σ) obtained from the fit, as per $FWHM = 2\sqrt{2\ln 2} \sigma$ (Fig. 3.3G) for the subset of timepoints where the Gaussian function could fit the data.

Curvature analysis

For curvature analysis (Fig. 3.4C,D), local radius of curvature (μm) was calculated by inscribing a circle through three points spaced by an interval of $1.5 \mu\text{m}$ along the spline using a custom Python script. This radius was used to calculate curvature ($1/\mu\text{m}$) by taking the inverse.

Statistical analysis

Data are reported as mean \pm SEM where indicated. All statistical testing was performed using the Python SciPy statistical package in Python. Two-sided Mann-Whitney U testing was used to compare independent samples while Wilcoxon signed-rank tests were used to compare paired data sets since we did not test whether assumptions for normality were met due to low sample size. Correlations were examined by calculating the Spearman rank-order correlation coefficient and no outliers were removed. Due to the technical challenges of these experiments, sample sizes are small. We used $p < 0.05$ as the threshold for statistical significance and have directly indicated in the figure and figure legend the p value and n, where n refers to the number of cells. We have therefore not performed statistical analysis for experiments with $n \leq 4$ (Fig. 3.3). No statistical methods were used to predetermine sample size. The experiments were not randomized.

ACKNOWLEDGEMENTS

We thank Le Paliulis for critical microneedle manipulation advice, and Alan Verkman's lab for the use of their microforge. We thank Alexey Khodjakov for the gift of PtK2 GFP-

α -tubulin and PtK1 PA-GFP- α -tubulin cell lines and Jagesh Shah for the gift of the PtK2 EYFP-Cdc20 cell line. We thank David Agard, Maya Anjur-Dietrich, Wallace Marshall, Tim Mitchison, Dave Morgan, Dan Needleman, Adair Oesterle, Ron Vale, Orion Weiner, and members of the Fred Chang and Dumont labs for helpful discussions.

This work was supported by NIH DP2GM119177, NIH R01GM134132, NSF CAREER 1554139, the NSF Center for Cellular Construction DBI-1548297, the Rita Allen Foundation and Searle Scholars' Program (S.D.), NSF Graduate Research Fellowships (A.F.L. and P.S.) and a UCSF Moritz-Heyman Discovery Fellowship and UCSF Lloyd Kozloff Fellowship (A.F.L.).

CHAPTER FOUR

CONCLUSION

Emergent Mechanics of the Kinetochore-Microtubule Interface

In this dissertation I have used the kinetochore-microtubule interface as a model system for asking how nanometer-scale cellular machines perform complex micron-scale mechanical functions. Despite a wealth of molecular knowledge of different kinetochore components, the underlying physical mechanisms that enable the kinetochore to robustly link dynamic microtubules to chromosomes for proper segregation of DNA during cell division remain underexplored. Improper kinetochore attachments can lead to aneuploidy, which can underlie cancer and birth defects [1,2,38,128]. Thus, understanding kinetochore function is key for developing a basic understanding of how cellular machines perform complex mechanical tasks, and may also illuminate ways in which these functions go awry in the context of disease. How the mammalian kinetochore's many proteins give rise to its emergent functions is a longstanding question in the field. In this dissertation, I have explored some of the key physical principles that underlie the robust grip at the kinetochore-microtubule interface.

First, in Chapter 2 I addressed the question of how the mammalian kinetochore binds and tracks polymerizing and depolymerizing microtubules using the essential load-bearing protein Hec1(Ndc80). While it was well characterized that phosphoregulation of Hec1 changes the kinetochore's affinity for microtubules, it was not known whether this regulation affected kinetochore's grip on polymerizing or depolymerizing microtubules or both since kinetochores are always coupled together before anaphase. I used laser ablation to trigger cellular pulling on mutant kinetochores and decouple kinetochore pairs, and thereby separately probe Hec1's role on dynamic microtubules. I found that Hec1 phosphoregulation tunes friction along polymerizing

microtubules, yet does not compromise the kinetochore's grip on depolymerizing microtubules. These data suggest a mechanism by which mechanical, not biochemical, specialization of Ndc80 at the kinetochore underlies its strong yet tunable grip that still enables coupling to the dynamic microtubules that power chromosome movement.

Second, in Chapter 3 I addressed the question of how the mammalian kinetochore-fiber responds to and remodels under sustained force. This question is at the heart of understanding how force-generating cellular structures can maintain their structure over time. Using microneedles to directly pull on kinetochore-fibers inside cells, I found that sustained force causes k-fibers to lengthen but remain connected to kinetochores by persistently favoring plus-end polymerization, rather than growing faster, and by preventing minus-end depolymerization. Thus, k-fibers protect overall spindle architecture by locally dissipating force at their dynamic ends. Exerting force on long timescales, I uncovered the spindles' weakest point – k-fibers can break in their center, rather than detaching from kinetochores or spindle poles which suggests the kinetochore-microtubule interface is stronger than the k-fiber bundle itself. This demonstrates a key principle for spindle homeostasis: different physical mechanisms of local force dissipation by dynamic k-fiber limit force transmission to preserve robust spindle structure over time.

Looking forward, approaches and thinking from engineering and systems biology will be key to defining these emergent “whole kinetochore” properties, and for uncovering their molecular bases and functions. Many of these properties remain poorly understood: for example, why do many species' kinetochores bind so many more microtubules than are mechanically required for moving chromosomes? Budding yeast

divide successfully with just one kinetochore-microtubule, fission yeast kinetochores bind four microtubules, while mammalian kinetochores bind 15-25 microtubules [3]. This work also raises many questions about the nature of the kinetochore-fiber as a complex cellular structure. What is the nature of cross-linking that allows k-fibers to respond as single mechanical units to force, given that they can also exhibit asynchronous plus-end structure [129,130]? How do cells regulate k-fiber composition over mitosis and how much occurs independently of kinetochore grip regulation (e.g. local kinetochore phosphatases versus global post-translational tubulin modifications)? The answers to these questions would have key implications for the mechanism of force production by k-fibers and provide new insight into the role k-fibers play in spindle mechanics. More broadly, they would enrich our understanding of the interplay between architecture, dynamics, and mechanics that enable cellular structures to robustly generate, respond to and withstand force to perform key mechanical functions for the cell.

Mechanical Insights Across Species

"In addition to experimenting with cell types that are widely used by investigators, we should remember that nature sometimes reveals her most well kept secrets through exaggerated displays found only in exotic cell types." – S. Inoue and T. Salmon [46]

We have much to learn about kinetochore structure-function relationships from studying both differences and similarities between kinetochores across the tree of life [131–133]. For example, studying kinetochores of different sizes [134] or that bind different numbers of microtubules can illuminate diverse strategies that have emerged under different evolutionary constraints to accomplish the same task of chromosome

segregation [123]. Much of our understanding of kinetochore mechanics has come from studying species with point (monocentric) kinetochores, yet many species have holocentric kinetochores [135,136] which face different challenges for grip and coordination of dynamics of microtubules that are spatially distant. Comparing the mechanical function of diverse kinetochore architectures may reveal new principles governing the mechanics of the kinetochore-microtubule interface.

New Tools and Approaches

To define and probe the kinetochore's emergent properties, we will need tools to physically and molecularly perturb the kinetochore with a new level of control, and to read out quantitative responses. For example, approaches to externally control force and dynamics ([92,137]) and to quantitatively rewire kinetochore and k-fiber composition (e.g. with optogenetics [138]) will allow us to directly measure force production and transmission across this interface and define the quantitative contribution of different molecular components to whole-kinetochore and, eventually whole-spindle, mechanical properties. Ultimately, the conceptual and experimental integration of kinetochore architecture, mechanics, and signal processing will be essential to understanding how this cellular machine achieves robust chromosome segregation each time a cell divides.

REFERENCES

1. Hassold, T., and Hunt, P. (2001). To err (meiotically) is human: The genesis of human aneuploidy. *Nat. Rev. Genet.* 2, 280–291.
2. Rajagopalan, H., and Lengauer, C. (2004). Aneuploidy and cancer. *Nature* 432, 338–341.
3. McEwen, B.F., Heagle, A.B., Cassels, G.O., Buttle, K.F., and Rieder, C.L. (1997). Kinetochores fiber maturation in PtK1 cells and its implications for the mechanisms of chromosome congression and anaphase onset. *J. Cell Biol.* 137, 1567–80.
4. Johnston, K., Joglekar, A., Hori, T., Suzuki, A., Fukagawa, T., and Salmon, E.D. (2010). Vertebrate kinetochore protein architecture: Protein copy number. *J. Cell Biol.* 189, 937–943.
5. Musacchio, A., and Desai, A. (2017). A Molecular View of Kinetochore Assembly and Function. *Biology (Basel)*. 6, 5.
6. Pesenti, M.E., Prumbaum, D., Auckland, P., Smith, C.M., Faesen, A.C., Petrovic, A., Erent, M., Maffini, S., Pentakota, S., Weir, J.R., *et al.* (2018). Reconstitution of a 26-Subunit Human Kinetochore Reveals Cooperative Microtubule Binding by CENP-OPQUR and NDC80. *Mol. Cell* 71, 923-939.e10.
7. Monda, J.K., and Cheeseman, I.M. (2018). The kinetochore–microtubule interface at a glance. *J. Cell Sci.* 131, jcs214577.
8. Valverde, R., Ingram, J., and Harrison, S.C.S.C. (2016). Conserved Tetramer Junction in the Kinetochore Ndc80 Complex. *Cell Rep.* 17, 1915–1922.
9. Magidson, V., Paul, R., Yang, N., Ault, J.G., O’Connell, C.B., Tikhonenko, I.,

- Mcewen, B.F., Mogilner, A., Khodjakov, A., O'Connell, C.B., *et al.* (2015). Adaptive changes in the kinetochore architecture facilitate proper spindle assembly. *Nat. Cell Biol.* *17*, 1134–1144.
10. O'Connell, C.B., Khodjakov, A., and McEwen, B.F. (2012). Kinetochore flexibility: creating a dynamic chromosome-spindle interface. *Curr. Opin. Cell Biol.* *24*, 40–7.
 11. Smith, C.A., McAinsh, A.D., and Burroughs, N.J. (2016). Human kinetochores are swivel joints that mediate microtubule attachments. *Elife* *5*, 3985–3998.
 12. Wynne, D.J., and Funabiki, H. (2015). Kinetochore function is controlled by a phospho-dependent coexpansion of inner and outer components. *210*, 899–916.
 13. Cheeseman, I.M., Chappie, J.S., Wilson-Kubalek, E.M., and Desai, A. (2006). The Conserved KMN Network Constitutes the Core Microtubule-Binding Site of the Kinetochore. *Cell* *127*, 983–997.
 14. DeLuca, J.G., Gall, W.E., Ciferri, C., Cimini, D., Musacchio, A., and Salmon, E.D. (2006). Kinetochore microtubule dynamics and attachment stability are regulated by Hec1. *Cell* *127*, 969–982.
 15. Suzuki, A., Badger, B.L., and Salmon, E.D. (2015). A quantitative description of Ndc80 complex linkage to human kinetochores. *Nat. Commun.* *6*, 8161.
 16. Yoo, T.Y., Choi, J.-M., Conway, W., Yu, C.-H., Pappu, R. V, and Needleman, D.J. (2018). Measuring NDC80 binding reveals the molecular basis of tension-dependent kinetochore-microtubule attachments. *Elife* *7*, e36392.
 17. Monda, J.K., Whitney, I.P., Tarasovetc, E. V., Wilson-Kubalek, E., Milligan, R.A., Grishchuk, E.L., and Cheeseman, I.M. (2017). Microtubule Tip Tracking by the Spindle and Kinetochore Protein Ska1 Requires Diverse Tubulin-Interacting

- Surfaces. *Curr. Biol.* 27, 3666-3675.e6.
18. Volkov, V.A., Huis in 't Veld, P.J., Dogterom, M., and Musacchio, A. (2018). Multivalency of NDC80 in the outer kinetochore is essential to track shortening microtubules and generate forces. *Elife* 7, e36764.
 19. Dudka, D., Noatynska, A., Smith, C.A., Liaudet, N., McAinsh, A.D., and Meraldi, P. (2018). Complete microtubule–kinetochore occupancy favours the segregation of merotelic attachments. *Nat. Commun.* 9, 2042.
 20. Kuhn, J., and Dumont, S. (2017). Spindle assembly checkpoint satisfaction occurs via end-on but not lateral attachments under tension. *J. Cell Biol.* 216, 1533–1542.
 21. Nicklas, R.B. (1983). Measurements of the force produced by the mitotic spindle in anaphase. *J. Cell Biol.* 97, 542–548.
 22. Grishchuk, E.L., Molodtsov, M.I., Ataulakhanov, F.I., and McIntosh, J.R. (2005). Force production by disassembling microtubules. *Nature* 438, 384–8.
 23. Zaytsev, A. V., Sundin, L.J.R., DeLuca, K.F., Grishchuk, E.L., and DeLuca, J.G. (2014). Accurate phosphoregulation of kinetochore-microtubule affinity requires unconstrained molecular interactions. *J. Cell Biol.* 206, 45–59.
 24. Helgeson, L.A., Zelter, A., Riffle, M., MacCoss, M.J., Asbury, C.L., and Davis, T.N. (2018). The human Ska complex and Ndc80 complex interact to form a load-bearing assembly that strengthens kinetochore-microtubule attachments. *PNAS* 115, 2740–2745.
 25. Auckland, P., Clarke, N.I., Royle, S.J., and McAinsh, A.D. (2017). Congressing kinetochores progressively load Ska complexes to prevent force-dependent

- detachment. *J. Cell Biol.* 216, 1623–1639.
26. Cheerambathur, D.K., Prevo, B., Hattersley, N., Lewellyn, L., Corbett, K.D., Oegema, K., and Desai, A. (2017). Dephosphorylation of the Ndc80 Tail Stabilizes Kinetochore-Microtubule Attachments via the Ska Complex. *Dev. Cell* 41, 424–37.
 27. Paweł Ł. Janczyk, Katarzyna A. Skorupka, Tooley, J.G., Matson, D.R., Kestner, C.A., West, T., Pornillos, O., and Stukenberg, P.T. (2017). Mechanism of Ska Recruitment by Ndc80 Complexes to Kinetochores. *Dev. Cell* 41, 438–49.
 28. Agarwal, S., Smith, K.P., Zhou, Y., Suzuki, A., McKenney, R.J., and Varma, D. (2018). Cdt1 stabilizes kinetochore–microtubule attachments via an Aurora B kinase–dependent mechanism. *J. Cell Biol.* 217, 3446–3463.
 29. Kern, D.M., Monda, J.K., Su, K.-C., Wilson-Kubalek, E.M., Cheeseman, I.M., Monda, J.K., Su, K.-C., Wilson-Kubalek, E.M., and Cheeseman, I.M. (2017). Astrin-SKAP complex reconstitution reveals its kinetochore interaction with microtubule-bound Ndc80. *Elife* 6, e26866.
 30. DeLuca, K.F., Lens, S.M.A., and DeLuca, J.G. (2011). Temporal changes in Hec1 phosphorylation control kinetochore-microtubule attachment stability during mitosis. *J. Cell Sci.* 124, 622–634.
 31. Chan, Y.W., Jeyaprakash, A.A., Nigg, E.A., and Santamaria, A. (2012). Aurora B controls kinetochore-microtubule attachments by inhibiting Ska complex-KMN network interaction. *J. Cell Biol.* 196, 563–571.
 32. DeLuca, K.F., Meppelink, A., Broad, A.J., Mick, J.E., Peersen, O.B., Pektas, S., Lens, S.M.A., and DeLuca, J.G. (2018). Aurora A kinase phosphorylates Hec1 to

- regulate metaphase kinetochore-microtubule dynamics. *J. Cell Biol.* *217*, 163–177.
33. Long, A.F., Udy, D.B., and Dumont, S. (2017). Hec1 Tail Phosphorylation Differentially Regulates Mammalian Kinetochore Coupling to Polymerizing and Depolymerizing Microtubules. *Curr. Biol.* *27*, 1692–1699.
 34. Dumont, S., Salmon, E.D., and Mitchison, T.J. (2012). Deformations within moving kinetochores reveal different sites of active and passive force generation. *Science* *337*, 355–358.
 35. Grishchuk, E.L. (2017). Biophysics of Microtubule End Coupling at the Kinetochore. In *Centromeres and Kinetochores*, B. E. Black, ed. (Springer), pp. 397–428.
 36. Betterton, M.D., and McIntosh, J.R. (2013). Regulation of chromosome speeds in mitosis. *Cell. Mol. Bioeng.* *6*, 418–430.
 37. Armond, J.W., Vladimirou, E., Erent, M., McAinsh, A.D., and Burroughs, N.J. (2015). Probing microtubule polymerisation state at single kinetochores during metaphase chromosome motion. *J. Cell Sci.* *128*, 1991–2001.
 38. Bakhoun, S.F., and Compton, D.A. (2012). Kinetochores and disease: Keeping microtubule dynamics in check! *Curr. Opin. Cell Biol.* *24*, 64–70.
 39. Bakhoun, S.F., Thompson, S.L., Manning, A.L., and Compton, D.A. (2009). Genome stability is ensured by temporal control of kinetochore–microtubule dynamics. *Nat. Cell Biol.* *11*, 27–35.
 40. Akiyoshi, B., Sarangapani, K.K., Powers, A.F., Nelson, C.R., Reichow, S.L., Arellano-Santoyo, H., Gonen, T., Ranish, J.A., Asbury, C.L., and Biggins, S.

- (2010). Tension directly stabilizes reconstituted kinetochore-microtubule attachments. *Nature* 468, 576–579.
41. King, J.M., and Nicklas, R.B. (2000). Tension on chromosomes increases the number of kinetochore microtubules but only within limits. *J. Cell Sci.* 113 Pt 21, 3815–3823.
 42. Maddox, P., Straight, A., Coughlin, P., Mitchison, T.J., and Salmon, E.D. (2003). Direct observation of microtubule dynamics at kinetochores in *Xenopus* extract spindles: implications for spindle mechanics. *J. Cell Biol.* 162, 377–382.
 43. Matos, I., Pereira, A.J., Lince-Faria, M., Cameron, L.A., Salmon, E.D., and Maiato, H. (2009). Synchronizing chromosome segregation by flux-dependent force equalization at kinetochores. *J. Cell Biol.* 186, 11–26.
 44. Ganem, N.J., and Compton, D.A. (2006). Functional Roles of Poleward Microtubule Flux During Mitosis. *Cell Cycle* 5, 481–485.
 45. Dorn, J.F., and Maddox, P.S. (2012). Kinetochore dynamics: How protein dynamics affect chromosome segregation. *Curr. Opin. Cell Biol.* 24, 57–63.
 46. Inoué, S., and Salmon, E.D. (1995). Force generation by microtubule assembly/disassembly in mitosis and related movements. *Mol. Biol. Cell* 6, 1619–1640.
 47. Khodjakov, A., and Rieder, C.L. (1996). Kinetochores moving away from their associated pole do not exert a significant pushing force on the chromosome. *J. Cell Biol.* 135, 315–327.
 48. Wan, X., Cimini, D., Cameron, L.A., and Salmon, E.D. (2012). The coupling between sister kinetochore directional instability and oscillations in centromere

- stretch in metaphase PtK1 cells. *Mol. Biol. Cell* 23, 1035–46.
49. Hill, T.L. (1985). Theoretical problems related to the attachment of microtubules to kinetochores. *Proc. Natl. Acad. Sci. U. S. A.* 82, 4404–4408.
 50. Cheeseman, I.M., and Desai, A. (2008). Molecular architecture of the kinetochore-microtubule interface. *Nat. Rev. Mol. Cell Biol.* 9, 33–46.
 51. Rago, F., and Cheeseman, I.M. (2013). Review series: The functions and consequences of force at kinetochores. *J. Cell Biol.* 200, 557–565.
 52. Sarangapani, K.K., and Asbury, C.L. (2014). Catch and release: how do kinetochores hook the right microtubules during mitosis? *Trends Genet.* 30, 150–159.
 53. Ciferri, C., Pasqualato, S., Screpanti, E., Varetta, G., Santaguida, S., Dos Reis, G., Maiolica, A., Polka, J., De Luca, J.G., De Wulf, P., *et al.* (2008). Implications for kinetochore-microtubule attachment from the structure of an engineered Ndc80 complex. *Cell* 133, 427–39.
 54. Guimaraes, G.J., Dong, Y., McEwen, B.F., and DeLuca, J.G. (2008). Kinetochore-microtubule attachment relies on the disordered N-terminal tail domain of Hec1. *Curr. Biol.* 18, 1778–1784.
 55. Powers, A.F., Franck, A.D., Gestaut, D.R., Cooper, J., Gracyzk, B., Wei, R.R., Wordeman, L., Davis, T.N., and Asbury, C.L. (2009). The Ndc80 kinetochore complex forms load-bearing attachments to dynamic microtubule tips via biased diffusion. *Cell* 136, 865–875.
 56. Zaytsev, A. V., Mick, J.E., Maslennikov, E., Nikashin, B., DeLuca, J.G., and Grishchuk, E.L. (2015). Multisite phosphorylation of the NDC80 complex gradually

- tunes its microtubule-binding affinity. *Mol. Biol. Cell* 26, 1829–1844.
57. Elting, M.W., Hueschen, C.L., Udy, D.B., and Dumont, S. (2014). Force on spindle microtubule minus ends moves chromosomes. *J. Cell Biol.* 206, 245–256.
 58. Sikirzhytski, V., Magidson, V., Steinman, J.B., He, J., Le Berre, M., Tikhonenko, I., Ault, J.G., McEwen, B.F., Chen, J.K., Sui, H., *et al.* (2014). Direct kinetochore-spindle pole connections are not required for chromosome segregation. *J. Cell Biol.* 206, 231–243.
 59. Mitchison, T.J. (1989). Polewards Microtubule Flux in the Mitotic Spindle : *J. Cell Biol.* 109, 637–652.
 60. Su, K.-C., Barry, Z., Schweizer, N., Maiato, H., Bathe, M., and Cheeseman, I.M. (2016). A Regulatory Switch Alters Chromosome Motions at the Metaphase-to-Anaphase Transition. *Cell Rep.* 17, 1728–1738.
 61. Skibbens, R. V., Rieder, C.L., and Salmon, E.D. (1995). Kinetochore motility after severing between sister centromeres using laser microsurgery: evidence that kinetochore directional instability and position is regulated by tension. *J. Cell Sci.* 108, 2537–2548.
 62. Ke, K., Cheng, J., and Hunt, A.J. (2009). The Distribution of Polar Ejection Forces Determines the Amplitude of Chromosome Directional Instability. *Curr. Biol.* 19, 807–815.
 63. Miller, M.P., Asbury, C.L., and Biggins, S. (2016). A TOG protein confers tension sensitivity to kinetochore-microtubule attachments. *Cell* 165, 1428–1439.
 64. Nicklas, R.B., and Staehly, C.A. (1967). Chromosome micromanipulation. I. The mechanics of chromosome attachment to the spindle. *Chromosoma* 21, 1–16.

65. Skibbens, R. V., and Salmon, E.D. (1997). Micromanipulation of chromosomes in mitotic vertebrate tissue cells: tension controls the state of kinetochore movement. *Exp. Cell Res.* 235, 314–324.
66. McNeill, P.A., and Berns, M.W. (1981). Chromosome behavior after laser microirradiation of a single kinetochore in mitotic PtK2 cells. *J. Cell Biol.* 88, 543–553.
67. McIntosh, J.R., Grishchuk, E.L., Mophew, M.K., Efremov, A.K., Zhudenkov, K., Volkov, V.A., Cheeseman, I.M., Desai, A., Mastronarde, D.N., and Ataullakhanov, F.I. (2008). Fibrils connect microtubule tips with kinetochores: a mechanism to couple tubulin dynamics to chromosome motion. *Cell* 135, 322–333.
68. Wang, H.-W., Long, S., Ciferri, C., Westermann, S., Drubin, D., Barnes, G., and Nogales, E. (2008). Architecture and Flexibility of the Yeast Ndc80 Kinetochore Complex.
69. Kudalkar, E.M., Scarborough, E.A., Umbreit, N.T., Zelter, A., Gestaut, D.R., Riffle, M., Johnson, R.S., MacCoss, M.J., Asbury, C.L., and Davis, T.N. (2015). Regulation of outer kinetochore Ndc80 complex-based microtubule attachments by the central kinetochore Mis12/MIND complex. *Proc. Natl. Acad. Sci.* 112, 5583–5589.
70. Umbreit, N.T., Gestaut, D.R., Tien, J.F., Vollmar, B.S., Gonen, T., Asbury, C.L., and Davis, T.N. (2012). The Ndc80 kinetochore complex directly modulates microtubule dynamics. *Proc. Natl. Acad. Sci. U. S. A.* 109, 16113–16118.
71. Suzuki, A., Badger, B.L., Haase, J., Ohashi, T., Erickson, H.P., Salmon, E.D., and Bloom, K.S. (2016). How the kinetochore harnesses microtubule force and

- centromere stretch to move chromosomes revealed by a FRET tension sensor within Ndc80 protein. *Nat. Cell Biol.* *18*, 382–392.
72. Sarangapani, K.K., Akiyoshi, B., Duggan, N.M., Biggins, S., and Asbury, C.L. (2013). Phosphoregulation promotes release of kinetochores from dynamic microtubules via multiple mechanisms. *Proc. Natl. Acad. Sci. U. S. A.* *110*, 7282–7287.
73. Lampert, F., Hornung, P., and Westermann, S. (2010). The Dam1 complex confers microtubule plus end-tracking activity to the Ndc80 kinetochore complex. *J. Cell Biol.* *189*, 641–649.
74. Tien, J.F., Umbreit, N.T., Gestaut, D.R., Franck, A.D., Cooper, J., Wordeman, L., Gonen, T., Asbury, C.L., and Davis, T.N. (2010). Cooperation of the Dam1 and Ndc80 kinetochore complexes enhances microtubule coupling and is regulated by aurora B. *J. Cell Biol.* *189*, 713–723.
75. Schmidt, J.C., Arthanari, H., Boeszoermenyi, A., Dashkevich, N.M., Wilson-Kubalek, E.M., Monnier, N., Markus, M., Oberer, M., Milligan, R.A., Bathe, M., *et al.* (2012). The Kinetochore-Bound Ska1 Complex Tracks Depolymerizing Microtubules and Binds to Curved Protofilaments. *Dev. Cell* *23*, 968–980.
76. Hanisch, A., Silljé, H.H.W., and Nigg, E.A. (2006). Timely anaphase onset requires a novel spindle and kinetochore complex comprising Ska1 and Ska2. *EMBO J.* *25*, 5504–5515.
77. Rieder, C.L. (1981). The structure of the cold-stable kinetochore fiber in metaphase PtK1 cells. *Chromosoma* *84*, 145–158.
78. McDonald, K.L., O’Toole, E.T., Mastronarde, D.N., and McIntosh, J.R. (1992).

- Kinetochores microtubules in PTK cells. *J. Cell Biol.* 118, 369–383.
79. Cassimeris, L., and Salmon, E.D. (1991). Kinetochores microtubules shorten by loss of subunits at the kinetochores of prometaphase chromosomes. *J. Cell Sci.* 98, 151–158.
 80. Mitchison, T., Evans, L., Schulze, E., and Kirschner, M. (1986). Sites of microtubule assembly and disassembly in the mitotic spindle. *Cell* 45, 515–527.
 81. Koshland, D.E., Mitchison, T.J., and Kirschner, M.W. (1988). Polewards chromosome movement driven by microtubule depolymerization in vitro. *Nature* 331, 499–504.
 82. Dogterom, M., Kerssemakers, J.W.J., Romet-Lemonne, G., and Janson, M.E. (2005). Force generation by dynamic microtubules. *Curr. Opin. Cell Biol.* 17, 67–74.
 83. Rieder, C.L., Davison, E.A., Jensen, L.C.W., Cassimeris, L., and Salmon, E.D. (1986). Oscillatory movements of monooriented chromosomes and their position relative to the spindle pole result from the ejection properties of the aster and half-spindle. *J. Cell Biol.* 103, 581–591.
 84. Skibbens, R. V., Skeen, V.P., and Salmon, E.D. (1993). Directional instability of kinetochores motility during chromosome congression and segregation in mitotic newt lung cells: A push-pull mechanism. *J. Cell Biol.* 122, 859–875.
 85. Oriola, D., Needleman, D.J., and Brugués, J. (2018). The Physics of the Metaphase Spindle. *Annu. Rev. Biophys* 47, 655–73.
 86. Elting, M.W., Suresh, P., and Dumont, S. (2018). The Spindle: Integrating Architecture and Mechanics across Scales. *Trends Cell Biol.* 28, 896–910.

87. De Brabander, M., Geuens, G., Nuydens, R., Willebrords, R., Aerts, F., De Mey, J., and McIntosh, J.R. (1986). Microtubule Dynamics during the Cell Cycle: The Effects of Taxol and Nocodazole on the Microtubule System of Pt K2 Cells at Different Stages of the Mitotic Cycle. *Int. Rev. Cytol.* *101*, 215–274.
88. Jaqaman, K., King, E.M., Amaro, A.C., Winter, J.R., Dorn, J.F., Elliott, H.L., McHedlishvili, N., McClelland, S.E., Porter, I.M., Posch, M., *et al.* (2010). Kinetochore alignment within the metaphase plate is regulated by centromere stiffness and microtubule depolymerases. *J. Cell Biol.* *188*, 665–79.
89. Alushin, G.M., Lander, G.C., Kellogg, E.H., Zhang, R., Baker, D., and Nogales, E. (2014). High-Resolution microtubule structures reveal the structural transitions in $\alpha\beta$ -tubulin upon GTP hydrolysis. *Cell* *157*, 1117–1129.
90. Nicklas, R.B. (1997). How cells get the right chromosomes. *Science* (80-). *275*, 632–637.
91. Lin, N.K.H., Nance, R., Szybist, J., Cheville, A., and Paliulis, L. V. (2018). Micromanipulation of Chromosomes in Insect Spermatocytes. *J. Vis. Exp.*, e57359.
92. Suresh, P., Long, A.F., and Dumont, S. (2019). Microneedle manipulation of the mammalian spindle reveals specialized, short-lived reinforcement near chromosomes. *BioRxiv*.
93. Udy, D.B., Voorhies, M., Chan, P.P., Lowe, T.M., and Dumont, S. (2015). Draft De Novo Transcriptome of the Rat Kangaroo Potorous tridactylus as a Tool for Cell Biology. *PLoS One* *10*, e0134738.
94. Civelekoglu-Scholey, G., He, B., Shen, M., Wan, X., Roscioli, E., Bowden, B., and

- Cimini, D. (2013). Dynamic bonds and polar ejection force distribution explain kinetochore oscillations in PtK1 cells. *J. Cell Biol.* *201*, 577–93.
95. Nicklas, R.B. (1988). The Forces that Move Chromosomes in Mitosis. *Ann. Rev. Biophys. Chem* *17*, 431–49.
96. Gorbsky, G.J., and Borisy, G.G. (1989). Microtubules of the kinetochore fiber turn over in metaphase but not in anaphase. *J. Cell Biol.* *109*, 653–662.
97. Cassimeris, L., Rieder, C.L., Rupp, G., and Salmon, E.D. (1990). Stability of microtubule attachment to metaphase kinetochores in PtK1 cells. *J. Cell Sci.* *96*, 9–15.
98. Zhai, Y., Kronebusch, P.J., and Borisy, G.G. (1995). Kinetochore microtubule dynamics and the metaphase-anaphase transition. *J. Cell Biol.* *131*, 721–734.
99. Begg, D.A., and Ellis, G.W. (1979). Micromanipulation studies of chromosome movement. I. Chromosome-Spindle Attachment and the Mechanical Properties of Chromosomal Spindle Fibers. *J. Cell Biol.* *82*, 542–554.
100. Nicklas, R.B., Kubai, D.F., and Hays, T.S. (1982). Spindle Microtubules and Their Mechanical Associations after Micromanipulation in Anaphase. *J. Cell Biol.* *95*, 91–104.
101. Gatlin, J.C., Matov, A., Danuser, G., Mitchison, T.J., and Salmon, E.D. (2010). Directly probing the mechanical properties of the spindle and its matrix. *J. Cell Biol.* *188*, 481–9.
102. Fong, K.K., Sarangapani, K.K., Yusko, E.C., Riffle, M., Llauró, A., Graczyk, B., Davis, T.N., and Asbury, C.L. (2017). Direct measurement of microtubule attachment strength to yeast centrosomes. *Mol. Biol. Cell* *28*, 1853–61.

103. Nicklas, R.B., Lee, G.M., Rieder, C.L., and Rupp, G. (1989). Mechanically cut mitotic spindles: clean cuts and stable microtubules. *J. Cell Sci.* *94 (Pt 3)*, 415–423.
104. Gittes, F., Mickey, B., Nettleton, J., and Howard, J. (1993). Flexural rigidity of microtubules and actin filaments measured from thermal fluctuations in shape. *J. Cell Biol.* *120*, 923–934.
105. Ward, J.J., Roque, H., Antony, C., and Nédélec, F. (2014). Mechanical design principles of a mitotic spindle. *Elife* *3*, e03398.
106. Schaedel, L., John, K., Gaillard, J., Nachury, M. V., Blanchoin, L., and Théry, M. (2015). Microtubules self-repair in response to mechanical stress. *Nat. Mater.* *14*, 1156–1163.
107. Spurck, T.P., Stonington, O.G., Snyder, J.A., Pickett-Heaps, J.D., Bajer, A., and Mole-Bajer, J. (1990). UV microbeam irradiations of the mitotic spindle. II. Spindle fiber dynamics and force production. *J. Cell Biol.* *111*, 1505–1518.
108. Portran, D., Schaedel, L., Xu, Z., Théry, M., and Nachury, M.V. (2017). Tubulin acetylation protects long-lived microtubules against mechanical ageing. *Nat. Cell Biol.* *19*, 391–398.
109. Vemu, A., Szczesna, E., Zehr, E.A., Spector, J.O., Grigorieff, N., Deaconescu, A.M., and Roll-Mecak, A. (2018). Severing enzymes amplify microtubule arrays through lattice GTP-tubulin incorporation. *Science* *361*, eaau1504.
110. McNally, F.J., and Roll-Mecak, A. (2018). Microtubule-severing enzymes: From cellular functions to molecular mechanism. *J. Cell Biol.* *217*, 4057–4069.
111. Gasic, I., and Mitchison, T.J. (2019). Autoregulation and repair in microtubule

- homeostasis. *Curr. Opin. Cell Biol.* *56*, 80–87.
112. Franck, A.D., Powers, A.F., Gestaut, D.R., Gonen, T., Davis, T.N., and Asbury, C.L. (2007). Tension applied through the Dam1 complex promotes microtubule elongation providing a direct mechanism for length control in mitosis. *Nat. Cell Biol.* *9*, 832–7.
 113. Long, A.F., Kuhn, J., and Dumont, S. (2019). The mammalian kinetochore–microtubule interface: robust mechanics and computation with many microtubules. *Curr. Opin. Cell Biol.* *60*, 60–67.
 114. Li, X., and Nicklas, R.B. (1995). Mitotic forces control a cell-cycle checkpoint. *Nature* *373*, 630–632.
 115. Dumont, S., and Mitchison, T.J. (2009). Compression regulates mitotic spindle length by a mechanochemical switch at the poles. *Curr. Biol.* *19*, 1086–95.
 116. Guild, J., Ginzberg, M.B., Hueschen, C.L., Mitchison, T.J., and Dumont, S. (2017). Increased lateral microtubule contact at the cell cortex is sufficient to drive mammalian spindle elongation. *Mol. Biol. Cell* *28*, 1975–1983.
 117. Ganem, N.J., Upton, K., and Compton, D.A. (2005). Efficient mitosis in human cells lacking poleward microtubule flux. *Curr. Biol.* *15*, 1827–32.
 118. Nicklas, R.B. (1967). Chromosome micromanipulation. II. Induced reorientation and the experimental control of segregation in meiosis. *Chromosoma* *21*, 17–50.
 119. Nicklas, R.B., and Koch, C.A. (1969). Chromosome micromanipulation. 3. Spindle fiber tension and the reorientation of mal-oriented chromosomes. *J. Cell Biol.* *43*, 40–50.
 120. Paliulis, L. V, and Nicklas, R.B. (2004). Micromanipulation of Chromosomes

- Reveals that Cohesion Release during Cell Division Is Gradual and Does Not Require Tension. *Curr. Biol.* *14*, 2124–2129.
121. Shimamoto, Y., and Kapoor, T.M. (2012). Microneedle-based analysis of the micromechanics of the metaphase spindle assembled in *Xenopus laevis* egg extracts. *Nat. Protoc.* *7*, 959–69.
 122. Itabashi, T., Takagi, J., Shimamoto, Y., Onoe, H., Kuwana, K., Shimoyama, I., Gaetz, J., Kapoor, T.M., and Ishiwata, S. (2009). Probing the mechanical architecture of the vertebrate meiotic spindle. *Nat. Methods* *6*, 167–172.
 123. Crowder, M.E., Strzelecka, M., Wilbur, J.D., Good, M.C., Von Dassow, G., and Heald, R. (2015). A comparative analysis of spindle morphometrics across metazoans. *Curr. Biol.* *25*, 1542–1550.
 124. Takagi, J., Sakamoto, R., Shiratsuchi, G., Maeda, Y.T., and Shimamoto, Y. (2019). Mechanically Distinct Microtubule Arrays Determine the Length and Force Response of the Meiotic Spindle. *Dev. Cell* *49*, 267–278.
 125. Sasaki, T., Matsuki, N., and Ikegaya, Y. (2012). Targeted axon-attached recording with fluorescent patch-clamp pipettes in brain slices.
 126. Schindelin, J., Arganda-Carreras, I., Frise, E., Kaynig, V., Longair, M., Pietzsch, T., Preibisch, S., Rueden, C., Saalfeld, S., Schmid, B., *et al.* (2012). Fiji: An open-source platform for biological-image analysis. *Nat. Methods* *9*, 676–682.
 127. Meijering, E., Dzyubachyk, O., and Smal, I. (2012). Methods for cell and particle tracking. In *Methods in Enzymology* (Academic Press Inc.), pp. 183–200.
 128. Cimini, D., Howell, B., Maddox, P., Khodjakov, A., Degraffi, F., and Salmon, E.D. (2001). Merotelic kinetochore orientation is a major mechanism of aneuploidy in

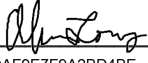
- mitotic mammalian tissue cells. *J. Cell Biol.* 152, 517–527.
129. VandenBeldt, K.J., Barnard, R.M., Hergert, P.J., Meng, X., Maiato, H., and McEwen, B.F. (2006). Kinetochores use a novel mechanism for coordinating the dynamics of individual microtubules. *Curr. Biol.* 16, 1217–23.
 130. Armond, J.W., Vladimirou, E., Erent, M., Mcainsh, A.D., and Burroughs, N.J. (2015). Probing microtubule polymerisation state at single kinetochores during metaphase chromosome motion. *J. Cell Sci.* 128, 1991–2001.
 131. Drinnenberg, I.A., Henikoff, S., Malik, H.S., and Akiyoshi, B. (2016). Evolutionary Turnover of Kinetochores: A Ship of Theseus? *Trends Cell Biol.* xx, 1–13.
 132. Drinnenberg, I.A., and Akiyoshi, B. (2017). Evolutionary Lessons from Species with Unique Kinetochores. In (Springer, Cham), pp. 111–138.
 133. Je Van Hooff, J., Tromer, E., van Wijk, L.M., Snel, B., and Kops, G.J. (2017). Evolutionary dynamics of the kinetochore network in eukaryotes as revealed by comparative genomics. *EMBO Rep.* 18, 1559–71.
 134. Drpic, D., Almeida, A.C., Aguiar, P., Renda, F., Damas, J., Lewin, H.A., Larkin, D.M., Khodjakov, A., and Maiato, H. (2018). Chromosome Segregation Is Biased by Kinetochore Size. *Curr. Biol.* 28, 1344-1356.e5.
 135. Drinnenberg, I.A., DeYoung, D., Henikoff, S., and Malik, H.S. (2014). Recurrent loss of CenH3 is associated with independent transitions to holocentricity in insects. *Elife* 3, e03676.
 136. Maddox, P.S., Oegema, K., Desai, A., and Cheeseman, I.M. (2004). “Holo”er than thou: Chromosome segregation and kinetochore function in *C. elegans*. *Chromosom. Res.* 12, 641–653.

137. Anjur-Dietrich, M.I., and Needleman, D.J. (2018). Mechanisms of force generation between chromosomes and microtubules in the mitotic spindle. *Mol Biol Cell* 28, P2055.
138. Zhang, H., Aonbangkhen, C., Tarasovetc, E. V, Ballister, E.R., Chenoweth, D.M., and Lampson, M.A. (2017). Optogenetic control of kinetochore function. *Nat. Chem. Biol.* 13, 1096–1101.

Publishing Agreement

It is the policy of the University to encourage open access and broad distribution of all theses, dissertations, and manuscripts. The Graduate Division will facilitate the distribution of UCSF theses, dissertations, and manuscripts to the UCSF Library for open access and distribution. UCSF will make such theses, dissertations, and manuscripts accessible to the public and will take reasonable steps to preserve these works in perpetuity.

I hereby grant the non-exclusive, perpetual right to The Regents of the University of California to reproduce, publicly display, distribute, preserve, and publish copies of my thesis, dissertation, or manuscript in any form or media, now existing or later derived, including access online for teaching, research, and public service purposes.

DocuSigned by:

DAF9E7F9A2BD4BE... Author Signature

3/4/2020
Date